SCIENCE CHINA
Physics, Mechanics & Astronomy

• Article •

January 2016 Vol. 00 No. 0: 000000
doi:

arXiv:1604.03662v2 [gr-qc] 23 Jul 2016

Tests of Gravitational Symmetries with Radio Pulsars

Lijing Shao[1,2] and Norbert Wex[3]

[1]*Max Planck Institute for Gravitational Physics (Albert Einstein Institute), Am Mühlenberg 1, D-14476 Potsdam-Golm, Germany*
[2]*School of Physics and State Key Laboratory of Nuclear Physics and Technology, Peking University, Beijing 100871, China*
[3]*Max-Planck-Institut für Radioastronomie, Auf dem Hügel 69, D-53121 Bonn, Germany*

Received January 1, 2016; accepted January 1, 2016; published online January 1, 2016

Symmetries play important roles in modern theories of physical laws. In this paper, we review several experimental tests of important symmetries associated with the gravitational interaction, including the universality of free fall for self-gravitating bodies, time-shift symmetry in the gravitational constant, local position invariance and local Lorentz invariance of gravity, and spacetime translational symmetries. Recent experimental explorations for post-Newtonian gravity are discussed, of which, those from pulsar astronomy are highlighted. All of these tests, of very different aspects of gravity theories, at very different length scales, favor to very high precision the predictions of the strong equivalence principle (SEP) and, in particular, general relativity which embodies SEP completely. As the founding principles of gravity, these symmetries are motivated to be promoted to even stricter tests in future.

Gravitation, Radio Pulsars, Spacetime Symmetry

PACS number(s): 04.80.Cc, 97.60.Gb, 11.30.-j

Citation: L. Shao and N. Wex, Sci. China-Phys. Mech. Astron., 00, 000000 (2016), doi:

1 Introduction

One hundred years ago, in November 1915, Albert Einstein presented the final form of his field equations of gravitation (without cosmological term) to the Prussian Academy of Science [1]. With this publication, general relativity (GR) was finally completed as a logically consistent physical theory. Already one week before, based on the vacuum form of his field equations, Einstein was able to demonstrate that GR naturally explains the anomalous advance of the Mercury perihelion [2]. Since then, GR was confronted with various dedicated ground- and space-based precision experiments [3]. GR has passed all these tests with flying colors, including the, since then much improved, initial three classical tests, namely the perihelion advance of Mercury, the deflection of light by the Sun, and the gravitational redshift. Various, quite diverse aspects of gravity are covered by GR: the (accelerated) expansion of the Universe, the reaction of the gravitational radiation of inspiralling binaries, the existence of black holes as the end products of gravitational collapse, the dragging of spacetime by a massive rotating body, the quantum phase evolution of cold atoms in the gravitational field, just to name a few. It is astonishing that a single gravity theory with only two parameters (namely the gravitational constant G and the cosmological constant Λ) is able to interpret all of these apparently vastly unrelated phenomena, to very high precision, at different length scales.

Nevertheless, there are various sophisticated reasons to search for gravity theories beyond Einstein's GR. Some of the most important ones are listed below.

- Einstein's GR does not employ quantum principles. Quantum nature of microscopic objects was well established to exquisite precision, and has already been integrated into our everyday life as a necessity. Quantum field theories that implement basic quantum ingredients describe all forces other than the gravity (namely, the electromagnetic force, the weak force, and the

© Science China Press and Springer-Verlag Berlin Heidelberg 2016

strong force), and they are tested against numerous data from particle accelerators, with many important predictions verified highly satisfactorily [4]. However, GR is known to have difficulties to be renormalized, which is one of the basic requirements for a modern quantum field theory.

- A related problem is about the appearance of singularities in spacetime in GR, under rather general circumstances. The singularity theorems of GR show that such singularities are inevitable in many physical situations [5]. There is hope that, by incorporating quantum fluctuations to GR, these singularity problems will be cured [6].

- During recent decades, new phenomena from astrophysics and cosmology ask for dark ingredients in our Universe (namely, dark matter and dark energy). Their gravitational behaviors are crucial in explaining continuously accumulating new observations. While these dark ingredients have not (yet) shown up as new particles in dedicated experiments in ground-based laboratories, some theories suggest to modify GR to avoid the need of dark matter and/or dark energy [7].

- Besides the aforementioned dark matter and dark energy, cosmological data are favoring an exponentially growing inflation era during the very early Universe. Such a scenario needs extra inputs beyond GR for the dynamics of spacetime, for example, one or several scalar inflatons that drive the exponential expansion. This might suggests a scalar degree in gravity, in addition to the canonical rank-2 metric tensor in GR [7].

Although an ultimate quantum gravity theory is still under construction, different modified gravity theories were built tentatively to account for one or several of the aforementioned problems. Scalar-tensor theories of gravity have been studied since the 1940s, with Jordan-Fierz-Brans-Dicke gravity as their most prominent representative (see Ref. [8], and references therein). An important motivation behind Jordan-Fierz-Brans-Dicke gravity was the promotion of G to a dynamical field, by this introducing a time-varying gravitational constant in an expanding Universe [9].

More elaborate gravity theories have been "designed" to address (at least parts of) the problem of the dark sector. One of the early attempts was Bekenstein's tensor-vector-scalar (TeVeS) theory, a covariant field theory in the modified Newtonian dynamics paradigm, aiming to explain dark matter as a manifest of a modification to GR [10, 11].

Hořava suggested different scaling indices for temporal and spatial components of a fossilized spacetime (that has a preferred time direction) to achieve a power-counting renormalizable, UV complete, gravity theory [12]. These new gravity theories were refined later by other authors to evade tensions with existing and upcoming experiments, and cure possible intrinsic problems in the theory [13].

As a general rule, new theories intend to break some foundational symmetries in GR. We are not to state that breaking these symmetries is necessarily bad, instead, these possibilities should be explored as clues to alternatives [14]. On top of that, this generally introduces a parameter space, in which GR can be tested [15, 16]. Nevertheless, from pure aesthetic viewpoint, a theory with less symmetry could be less appealing. Extending GR with quantum principles is widely believed to require deep insights into GR's founding principles and possibly do some modification/generalization/extension to them. Ultimately, one should resort to discriminating experiments to judge between different choices of theories. Therefore, experimentally exploring the foundational symmetries in GR is highly desired.

Speaking of foundational symmetries, the *strong equivalence principle* (SEP) represents a highly condensed wisdom for GR [17]. Based on early work by Robert Dicke, Clifford Will nicely constructed and popularized SEP with three ingredients [3, 15] (see also the discussion in Ref. [18]):

- Validity of the weak equivalence principle for test particles (WEP) is extended to self-gravitating bodies (GWEP). It means that in the external gravitational field, bodies of negligible or non-negligible self-gravity should fall at the same rate, regardless of the detailed composition (for example, with different number of quarks and electrons, different fraction ε of gravitational binding energy, et cetera). It is a nontrivial extension of Galileo's universality of free fall to include also bodies where the gravitational binding contributes a significant fraction to their mass, e.g. the Sun ($\varepsilon \sim 10^{-6}$) or neutron stars ($\varepsilon \sim 0.1$).

- Local Lorentz invariance in gravity. It states that, no matter of the velocity of experimental apparatus, the outcome of local experiments, gravitational or non-gravitational, should be described by the same set of physical laws.

- Local position invariance in gravity. It states that, no matter of when and where the local experiments are performed, the outcome should be interpreted by the same set of physical laws.

The SEP describes the general rules for the outcome of experiments, both gravitational and non-gravitational. It is indeed lying to the heart of GR. Actually, there are good arguments that GR is the only valid gravity that respects SEP in its entirety [3]. Therefore, probing the building blocks of SEP probes the deep foundational principles/symmetries of GR.

In this review, we will touch on some experimental tests on different aspects of SEP. Precision pulsar timing experiments are highlighted, because they not only provide the most limiting constraints in most areas, but also probe certain aspects of strong-field gravity, in particular those associated with neutron stars, the supposedly most compact mate-

rial bodies in nature [19, 20]. In the next section, the universality of free fall for self-gravitating bodies is reviewed, with a focus on experiments that constrain the violation of GWEP in the quasi-stationary strong-field regime. Closely related to a violation of GWEP is the existence of dipolar radiation, in particular if the modification of GR is associated with additional "gravitational charges". This is a powerful discriminant in asserting the principle from orbital decays of binary pulsars, capable of capturing deviations from GR that evade free-fall tests. In Section 3 and Section 4, the local position invariance and local Lorentz invariance in gravity are examined in two generic, overlapping but not equivalent, frameworks for post-Newtonian gravity, namely, the parametrized post-Newtonian (PPN) formalism [3] and the standard-model extension (SME) [21]. Again, pulsar timing turns out one of the best testbeds for any tiny deviations from GR permitted by these two frameworks. In Section 5, we review results on energy-momentum conservation laws in post-Newtonian gravity in the PPN formalism [15]. Finally, in Section 6 we briefly look into aspects of a time-varying gravitational constant, whereby we underline the complementary aspect of pulsar tests. Section 7 summarizes the paper, and gives a short discussion on possible strong-field effects and the upcoming gravitational-wave experiments [22, 23].

2 Universality of Free Fall for Self-Gravitating Bodies

As mentioned in Section 1, SEP extends WEP to the gravitational WEP (GWEP), i.e. the universality of free fall for self-gravitating bodies. In GR, GWEP is fulfilled, i.e. in GR the world line of a body is independent of its chemical composition and gravitational binding energy. Therefore, a detection of a violation of GWEP, one of the three pillars of SEP (see Sec. 1), would directly falsify GR. On the other hand, alternative theories of gravity generally violate GWEP. This is also the case for most metric theories of gravity, which by definition fulfill WEP [15]. For a weakly self-gravitating body in a weak external gravitational field one can simply express a violation of GWEP as a difference between inertial (I) and (passive) gravitational (G) mass that is proportional to the gravitational binding energy, $E_{\rm grav}$, of the body,

$$\frac{m_{\rm G}}{m_{\rm I}} \simeq 1 + \eta_{\rm N} \frac{E_{\rm grav}}{m_{\rm I} c^2} = 1 + \eta_{\rm N}\, \varepsilon \,. \qquad (1)$$

The Nordtvedt parameter $\eta_{\rm N}$ is a theory dependent constant. In the parameterized post-Newtonian (PPN) framework, $\eta_{\rm N}$ is given as a combination of different PPN parameters (see Ref. [15] for details). As a consequence of Eq. (1), the Earth ($\varepsilon \approx -5 \times 10^{-10}$) and the Moon ($\varepsilon \approx -2 \times 10^{-11}$) would fall differently in the gravitational field of the Sun (Nordtvedt effect [24]). The parameter $\eta_{\rm N}$ is therefore tightly constrained by the lunar-laser-ranging (LLR) experiments to $\eta_{\rm N} = (3.0 \pm 3.6) \times 10^{-4}$, which is in perfect agreement with $\eta_{\rm N} = 0$, the prediction of GR [25].

In view of the smallness of the fractional self-gravity of Earth and Moon, the LLR experiment says nothing about strong-field aspects of GWEP. GWEP could still be violated for extremely compact objects, like neutron stars ($\varepsilon \sim 0.1$), meaning that a neutron star would feel a quite different acceleration in an external gravitational field than a weakly self-gravitating body. Since beyond the first post-Newtonian approximation there is no general PPN formalism available, and Eq. (1) is not applicable for strongly self-gravitating masses, discussions of GWEP violation in this regime are best done within theory-specific frameworks. A particularly suitable framework that nicely allows the study of various strong-field deviations from GR, is the two-parameter class of mono-scalar-tensor theories $T_1(\alpha_0, \beta_0)$ of Refs. [26, 27], where the scalar field is sourced by the trace of the energy-momentum tensor. In this extension of the Jordan-Fierz-Brans-Dicke theory, the coupling strength is a (linear) function of the scalar field, $\alpha(\varphi) = \alpha_0 + \beta_0(\varphi - \varphi_0)$, with φ_0 being the asymptotic value of the scalar field φ. Jordan-Fierz-Brans-Dicke theory is recovered for $\beta_0 = 0$. As discovered by Damour and Esposito-Farèse, in such theories, for certain (negative) values of β_0, one finds significant strong-field deviations from GR, and a correspondingly strong violation of GWEP for neutron stars. To illustrate this violation of GWEP, it is sufficient to look at the leading order "Newtonian" terms in the equations of motion of a three body system, with masses m_A at (coordinate) locations $\mathbf{r}_A$ ($A = 1, 2, 3$) [28],

$$\ddot{\mathbf{r}}_A = -\sum_{B \neq A} \mathcal{G}_{AB} m_B \frac{\mathbf{r}_A - \mathbf{r}_B}{|\mathbf{r}_A - \mathbf{r}_B|^3} \,, \qquad (2)$$

where the body-dependent effective gravitational constant $\mathcal{G}_{AB}$ is related to the Newtonian gravitational constant G (as measured in a Cavendish-type experiment) by

$$\mathcal{G}_{AB} = G\, \frac{1 + \sigma_A \sigma_B}{1 + \alpha_0^2} \,. \qquad (3)$$

The quantity σ_A denotes the effective scalar coupling of mass m_A, which gives the total scalar charge of body A by $\omega_A = -\sigma_A m_A$. For weakly self-gravitating bodies $\sigma_A \simeq \alpha_0$. σ_A is a body-dependent quantity, in general different for masses with different gravitational binding energy. In other words, the gravitational interaction depends on the internal structure of the bodies, and therefore GEWP is violated. In GR on the other hand, one can introduce one effective mass, due to the effacement of the internal structure [29], leading to a universality of free fall for self-gravitating bodies.

Eq. (2) implies that, two components of a binary system, say m_1 and m_2, will fall differently in the external field of a distant ($|\mathbf{r}_3| \gg |\mathbf{r}_1|, |\mathbf{r}_2|$) third body m_3, since the accelerations caused by the external mass are

$$\ddot{\mathbf{r}}_1^{\rm ext} \simeq \frac{1 + \sigma_1 \sigma_3}{1 + \alpha_0^2}\, \mathbf{g}^{\rm ext} \quad \text{and} \quad \ddot{\mathbf{r}}_2^{\rm ext} \simeq \frac{1 + \sigma_2 \sigma_3}{1 + \alpha_0^2}\, \mathbf{g}^{\rm ext} \,, \qquad (4)$$

respectively, where $\mathbf{g}^{\rm ext} \equiv G m_3 \mathbf{r}_3 / r_3^3$. The violation of GWEP

can therefore be written as

$$\Delta \cdot \mathbf{g}^{\rm ext} \equiv \ddot{\mathbf{r}}_1^{\rm ext} - \ddot{\mathbf{r}}_2^{\rm ext} \simeq (\sigma_1 - \sigma_2)\sigma_3 \cdot \mathbf{g}^{\rm ext} \,. \tag{5}$$

In the final step, we have used the fact that, Solar system experiments already imply $\alpha_0^2 \ll 1$.

For neutron stars, depending on β_0 and their masses, σ_A can deviate significantly from α_0. In fact, even for $\alpha_0 = 0$, σ_A can in principle be of order unity due to spontaneous scalarization [26]. Figure 1 shows σ_A as a function of the fractional gravitational binding energy of a neutron star for specific values of β_0. From this, one clearly sees the strong non-linearity of the violation of GWEP in the strong-field regime of these specific theories of gravity.

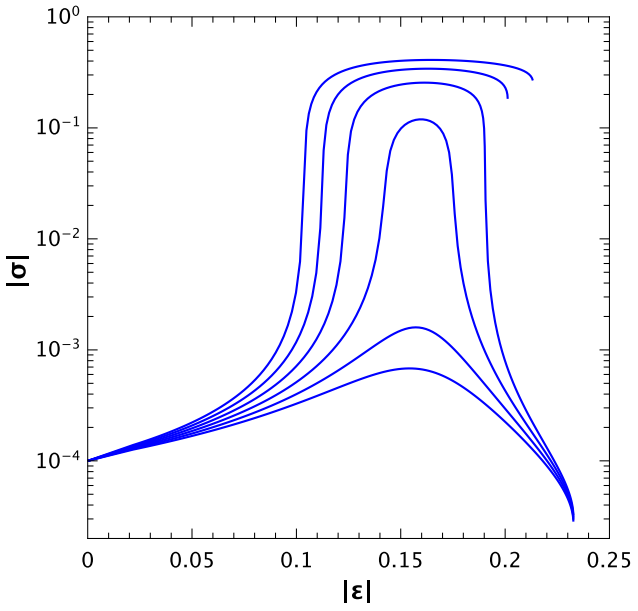

Figure 1 Effective scalar coupling σ as a function of the fractional binding energy ε of a (stable) neutron star, for $T_1(\alpha_0, \beta_0)$ scalar-tensor theories of gravity. To calculate the blue lines, $\alpha_0 = 10^{-4}$ and $\beta_0 = -4.0$ (bottom), -4.2, -4.4, -4.6, -4.8, and -5.0 (top) was used. Furthermore, equation of state AP4 (as in Ref. [30]) was assumed, when calculating the structure of the neutron stars. As one can see, if β_0 is not too negative, then neutron stars tend to descalarize when approaching their maximum mass (cf. Ref. [31]).

For such strong-field aspects of GWEP, the best current tests do come from the timing observations of millisecond pulsars in wide orbits with white dwarf companions. If there is a violation of GWEP associated with the strong internal gravity of neutron stars, then the gravitational field of the Milky Way at the location of the pulsar (typically $|\mathbf{g}^{\rm ext}| \approx 2 \times 10^{-8}\,{\rm cm\,s^{-2}}$) would polarize the binary orbit in a characteristic way [32], causing, most importantly, a gradual periodic change of the orbital eccentricity (gravitational Stark effect). Currently, the best limits on Δ for neutron stars are obtained from the so-called Damour-Schäfer test, which is based on probabilistic considerations for small-eccentricity binary pulsars [32]. In such binary systems, the observed eccentricity is a combination of the forced eccentricity $\mathbf{e}_{\rm F}$ (in direction of the projected $\mathbf{g}^{\rm ext}$) and an intrinsic eccentricity $\mathbf{e}_{\rm R}$, that has a fixed length and rotates in the orbital plane with the frequency of the relativistic periastron advance $\dot{\omega}$ (analogue to Figure 5 below). For a binary, with orbital frequency n_b and semi-major axis a one finds

$$\mathbf{e}_{\rm F} = \frac{3\Delta}{2an_b\dot{\omega}}\,\mathbf{g}_{\perp}^{\rm ext} \,. \tag{6}$$

Consequently, the wider the orbit the stronger the polarizing effect would be. Note however, if $\dot{\omega}$ becomes comparable to the rotation of the system in the Galaxy, then Eq. (6) can no longer be applied, as the underlying assumptions for its derivation break down.

By statistically excluding (near) alignment between $\mathbf{e}_{\rm F}$ and $\mathbf{e}_{\rm R}$, one can generically place limits on $|\mathbf{e}_{\rm F}|$, and therefore on Δ, without knowledge of the actual length of $\mathbf{e}_{\rm R}$. Combining a whole population of pulsar – white dwarf systems, Stairs et al. [33] have obtained the so far best limit for a violation of GWEP by a strongly self-gravitating body,[1]

$$|\Delta| < 0.0056 \quad (95\%\ {\rm CL}) \,. \tag{7}$$

In view of Eq. (5), this limit however is not very constraining. For the white dwarf and the Galactic field $\sigma_2 \simeq \sigma_3 \simeq \alpha_0$, resulting in a weak limit on $|\sigma_1 - \alpha_0|$ for a neutron star since $|\alpha_0| \ll 1$.

There is an underlying assumption in the Damour-Schäfer test when combining multiple systems, which is related to the mass dependence of a GWEP violation. Constraining a Δ from a set of pulsar – white dwarf systems in a generic way requires the assumption that Δ is practically independent of the mass of the neutron star, as these systems have different pulsar masses. Even in the absence of non-perturbative behavior, one finds rather large deviations from that assumption along the range of observed neutron star masses. In the presence of non-perturbative strong-field effects, like the spontaneous scalarization mentioned above (see Figure 1), this assumption is not applicable at all. For this reason it is desirable to have direct tests, i.e. tests based on long term timing observations of individual systems with well known masses, where one directly constrains $\dot{e}$ (see Ref. [35] for details). As it requires a number of conditions to be met, like high timing precision and knowledge of the orbital orientation, only few systems turn out to be suitable at present. In Ref. [35] two binary pulsar systems have been identified as particularly suitable for a direct test of a GWEP violation, PSRs J1713+0747 and J1903+0327. While the work on PSR J1713+0747 is still in progress, preliminary results for PSR J1903+0327 have been published in Ref. [35], giving a rather weak constraint of $|\Delta| < 0.1$. Although this test will improve with time, through continuous timing, it will soon become mostly obsolete, because of a recent discovery of PSR J0337+1715, which is a

[1] Note, the limit in Ref. [34] is flawed, as explained in Ref. [20].

member of a hierarchical triple system [36]. In this system we have a 1.44 $M_\odot$ pulsar in a 1.63-day orbit with a 0.2 $M_\odot$ white dwarf. This inner binary is in a 327-day orbit with a 0.4 $M_\odot$ white dwarf, and consequently experiences an external acceleration $|\mathbf{g}^{\rm ext}| \sim 0.2\,{\rm cm\,s^{-2}}$, which is seven orders of magnitude larger than the one of the Galactic gravitational field given above. Consequently, PSR J0337+1715 might soon allow for a significantly improved limit on Δ. As already argued in Ref. [35], pulsars in hierarchical triple systems would be the ideal laboratories for testing GWEP, as they combine a strong external field $\mathbf{g}^{\rm ext}$ with a large fractional binding energy ε. In fact, simulations in Ref. [37] indicate that a limit of $|\Delta| \lesssim 10^{-7}$ might soon be achievable. Based on mock data simulations, Berti et al. [14] have demonstrated the potential of PSR J0337+1715 to constrain scalar-tensor theories, in particular with the timing capabilities of future radio telescopes, like the Square Kilometre Array (SKA).

There are, however, limitations to what in terms of GWEP violation can be tested with PSR J0337+1715. For instance, if gravity only deviates (significantly) from GR in the strong field regime, and hence the white dwarfs do not develop any relevant additional gravitational charges, then PSR J0337+1715 does not provide any (relevant) constraints. To illustrate this, let us look at those $T_1(\alpha_0,\beta_0)$ theories that exhibit spontaneous scalarization in the strong gravity of a neutron star. In such a case we find for the two white dwarfs $\sigma_2 = \sigma_3 = 0$, which leads to $\mathcal{G}_{12} = \mathcal{G}_{13} = \mathcal{G}_{23} = G$, no matter how strongly the pulsar (m_1) is scalarized (see discussion in Ref. [35]). Since $\sigma_3 = 0$, one finds $\Delta = 0$ from Eq. (5). An obvious other "blind-spot" of such a GWEP test is the situation where $\sigma_1 \simeq \sigma_2$ (cf. Eq. (5)). Indeed, in $T_1(\alpha_0,\beta_0)$ there is always a value for β_0, depending on the mass of the neutron star, where $\sigma_1 = \sigma_2$. Another example is Bekenstein's TeVeS theory [10], where neutron stars and white dwarfs do have the same effective scalar coupling [38].

Fortunately, there are other consequences of a violation of SEP, which are closely related to a violation of the universality of free fall of self-gravitating masses, and can be used as a test to overcome these gaps. One is the modification of the moment-of-inertia of the spinning pulsar, as it moves on an eccentric orbit around its companion. Such a consequence has generically been well constrained with the help of the double pulsar [39]. The other consequence of a violation of GWEP is a modification of the gravitational-wave damping in a binary pulsar system. In general, these modifications introduce a dipolar component, affecting the equations of motion already at the 1.5 post-Newtonian level, i.e. $(c/v_{\rm orb})^2$ times higher than the quadrupolar contribution in GR, where $v_{\rm orb}$ is the characteristic velocity of binary motion [15]. But even in the absence of a dipolar contribution, there is still a modification at the 2.5 post-Newtonian level (see Ref. [40] for the equations of motion in scalar-tensor theories). The most important consequence in binary pulsars, related to these modifications, is a change in the orbital period decay rate, $\dot{P}_b$. In particular systems which show a high asymmetry in compactness should be affected, as there one generally would expect a dominating dipolar contribution. Within the $T_1(\alpha_0,\beta_0)$ class of gravity theories, to give a concrete example, one finds

$$\dot{P}_b \simeq -\frac{4\pi^2}{P_b}\,\frac{G}{c^3}\,\frac{m_1 m_2}{M}\,\frac{1+e^2/2}{(1-e^2)^{5/2}}\,(\sigma_1-\sigma_2)^2 + O(c^{-5})\,. \quad (8)$$

If the companion is a white dwarf, then $\sigma_2 \simeq \alpha_0 \ll 1$. There are quite a few pulsar – white dwarf systems that can be utilized to constrain σ_1 via a $\dot{P}_b$ measurement. As σ_1 is highly mass dependent, it is important to perform such a test for different pulsar masses. The best such constraints to date are (95% confidence, sorted according to pulsar mass),

- PSR J1141−6545 (1.27 $M_\odot$): $|\sigma_1 - \alpha_0| < 0.004$ [41],
- PSR J1738+0333 (1.46 $M_\odot$): $|\sigma_1 - \alpha_0| < 0.002$ [38],
- PSR J1909−3744 (1.54 $M_\odot$): $|\sigma_1 - \alpha_0| < 0.008$,
- PSR J1012+5307 ($\sim$ 1.7 $M_\odot$): $|\sigma_1 - \alpha_0| < 0.008$ [42],
- PSR J0348+0342 (2.01 $M_\odot$): $|\sigma_1 - \alpha_0| < 0.005$ [43].

For simplicity, we have omitted the error on the pulsars' masses in the above list. The limit for PSR J1909−3744 has been derived here for the first time, based on the timing results recently published in Ref. [44]. Although we have used a particular class of scalar-tensor theories, to illustrate the physics behind these tests, the limits above can be seen more generically as limits on any difference in gravitational charges, which leads to a rotating gravitational dipole [45]. In Refs. [46-48] this has been used to constrain two particular classes of vector-tensor theories of gravity, that violate boost invariance in the gravitational sector. More details are given in Section 4.

3 Local Position Invariance

Ernst Mach's concept of inertia was an important guiding factor in Einstein's development of GR, and it was given a name, *Mach's principle* [49]. The statement of Mach's principle is rather vague and generally understood as that *inertia originates in a kind of interaction between bodies* [17] or *local physical laws are determined by the large-scale structure of the universe* [5]. In terms of gravity theories, GR, although influenced by Mach's principle, is not fully Machian — and to some extent even appears anti-Machian [50] — while, for example, the Jordan-Fierz-Brans-Dicke theory [9, 51, 52] and its generalizations [26-28], with an effective gravitational constant depending on spacetime via a scalar field, are more Machian [53]. Bondi and Samuel listed eleven versions of Mach's principle, numbered as Mach0 to Mach10 [54], wherein Mach1, Mach3, and Mach6 are directly relevant to the topic here.

Although we are not necessarily saying that Mach's principle is correct, nevertheless, it provides interesting ideas, stimulating the exploration of gravity theories. Especially the idea that the local gravitational law is influenced by the

universal matter distribution was considered by many authors [15,52,55-59]. As we know from cosmology, the distribution of matter is uniform and isotropic only to a certain degree of approximation. If Mach's principle holds in a strong sense, we might expect that the slight asymmetries in the distribution at large would result in a slight anisotropy in the gravitational law [60,61]. In other words, the law to interpret gravitational experiments will depend on where the experiments are performed, with the local position invariance of gravity violated. Such a possibility is studied below in the context of post-Newtonian gravity.

We concentrate on one of the ten PPN parameters which characterizes a possible anisotropy in the gravitational interaction of localized systems due to the universal matter distribution. Such an anisotropy is described by the Whitehead parameter, ξ, in the post-Newtonian limit [3,15]. The n-body Lagrangian has a ξ-term through three-body interactions (see Eq. (6.80) in Ref. [15]),

$$L_\xi = -\frac{\xi}{2}\frac{G^2}{c^2}\sum_i\sum_{j\neq i}\frac{m_i m_j}{r_{ij}^3}\mathbf{r}_{ij}\cdot\left[\sum_k m_k\left(\frac{\mathbf{r}_{jk}}{r_{ik}}-\frac{\mathbf{r}_{ik}}{r_{jk}}\right)\right]. \quad (9)$$

In the discussions below, the major contribution of the third body comes from our Galaxy [15, 59, 62].[2] We consider a system that the Galactic center lies in its direction of $\mathbf{n}_\mathrm{G}$ and at a distance of R_G. We will assume that the matter in the Galaxy is concentrated at the Galactic center. It was calculated explicitly that such an assumption, compared with the extended matter distribution in reality (with the bulge, the disk and the dark matter halo), introduces a correction factor of about two [59,62].

The phenomena of local position invariance violation, introduced by the dynamics deduced from Eq. (9), include anomalous Earth tides, anomalous advance rate in planetary perihelion [15,57], anomalous precession of a circular binary orbit [63], and anomalous precession of a massive body's spin [62,64].

Anomalous Earth Tides. When discussing Earth tides, it is convenient to attribute the violation in local position invariance, characterized by ξ in the PPN formalism, to an effectively anisotropic gravitational constant (see Eq. (6.75) in Ref. [15]),

$$\begin{aligned} G_\mathrm{local} &= G_0\left[1+\xi\,(\mathbf{e}\cdot\mathbf{n}_\mathrm{G})^2\left(1-\frac{3I_\oplus}{M_\oplus R_\oplus^2}\right)U_\mathrm{G}\right. \\ &\quad \left.+\xi\,(\mathbf{e}\cdot\mathbf{n}_\odot)^2\left(1-\frac{3I_\oplus}{M_\oplus R_\oplus^2}\right)U_\odot\right], \end{aligned} \quad (10)$$

where $I_\oplus$, $M_\oplus$, and $R_\oplus$ are the moment of inertia, mass and radius of the Earth, respectively, G_0 is the bare gravitational constant,[3] and $\mathbf{e}$ is the unit vector pointing from the center of the Earth to the location where G is being measured [15]. The changing of $\mathbf{e}$, due to the Earth's rotation, and the changing of $\mathbf{n}_\odot$, due to the Earth's revolving around the Sun, make the gravitational interaction change at specific frequencies with characteristic phases [57].

Will [15] summarized the primary effects of Eq. (10) on the local gravitational acceleration: i) semi-diurnal variations with periods around 12 hours, ii) diurnal variations with periods around 24 hours, iii) long-period zonal variations with periods of one-half year or one year, iv) long-period spherical variations with a period of one year that, in contrast to the other three, have no dependence on the latitude. These phenomena were called *Earth's tides*, and could be studied with gravimeter [15, 57, 65]. Warburton and Goodkind used data from superconducting gravimeters and obtained a limit of $|\xi| \lesssim 10^{-3}$ [66]. New developments in superconducting gravimeter networks are expected to probe ξ at the level of 10^{-5} [67].

Anomalous Advance of Planetary Perihelion. In the case of two-body problem, Eq. (9) produces an extra acceleration between masses m_1 and m_2 (see Eq. (8.73) in Ref. [15] with a different sign convention),

$$\mathbf{a}_\xi = \xi\frac{U_\mathrm{G}}{c^2}\frac{G(m_1+m_2)}{r^2}\left[2(\mathbf{n}_\mathrm{G}\cdot\mathbf{n})\mathbf{n}_\mathrm{G}-3\mathbf{n}\,(\mathbf{n}_\mathrm{G}\cdot\mathbf{n})^2\right], \quad (11)$$

where r is the coordinate separation, and $\mathbf{n}$ is the unit vector of relative position. Such an acceleration contributes to the advance rates of planetary perihelion (see Eq. (25) in Ref. [57] for the expression). Numerically, for Mercury one has an anomalous advance rate [15],

$$\delta\dot{\omega}_\mathrm{☿} \simeq 63\,\xi \quad \text{arcsec century}^{-1}, \quad (12)$$

while its general-relativistic advance rate is 43 arcsec century^{-1}. Because that, on one hand, other PPN parameters also have contribution to the advance rate, and on the other hand, the measurement precision of $\dot{\omega}$ is limited, ξ can not be constrained tightly from the anomalous advance of planetary perihelion [15].

Anomalous Orbital Precession of Binary Pulsars. It was shown that for circular orbits, Eq. (11) would lead to a precession of the orbital norm, around the direction of the binary's acceleration towards the Galactic center, $\mathbf{n}_\mathrm{G}$ [63]. In pulsar timing, such a precession causes a change in our viewing of the binary orbit, that results in a nonzero drift in the projected semi-major axis of the pulsar orbit, $x \equiv a_p \sin i/c$, due to a varying inclination angle i. Therefore, with the fitting parameter $\dot{x}$ from times of arrival of pulse signals, the ξ parameter can be constrained. However, the full geometric orientation of the binary orbit is required in the calculation, while unfortunately the longitude of ascending node, Ω, is in general not an observable in pulsar timing [68]. With a probabilistic assumption that Ω is uniformly picked from $[0°, 360°)$ in the sense of a *nuisance parameter* in Bayes'

[2] For the case of Earth tides, the second major contribution, from the Sun, is also included. The relative strengths are characterized by the gravitational potentials at the location of the Earth, with $U_\mathrm{G}/c^2 \sim 5\times10^{-7}$ for the Galaxy and $U_\odot/c^2 \sim 1\times10^{-8}$ for the Sun [15].

[3] We have renormalized G_0 with an isotropic term, $\xi(3 + I/MR^2)(U_\mathrm{G} + U_\odot)$, that is irrelevant to the discussions here.

priors, the following limit was obtained by combining observations from PSRs J1012+5307 and J1738+0333 at 95% confidence level [63],

$$|\xi| < 3.1 \times 10^{-4} \,. \tag{13}$$

In calculating the above limit, an assumption that ξ has only weak dependence on the component masses of binary pulsars was made.

Anomalous Spin Precession of the Sun. Nordtvedt considered Eq. (9) in the case of extended bodies. He showed that an isolated massive star, with internal equilibrium, undergoes a free spin precession around its Galactic acceleration towards the Galactic center, with an angular frequency [64],

$$\Omega^{\xi} = \xi \left(\frac{2\pi}{P}\right) U_{\rm G} \cos\psi \,, \tag{14}$$

where P is the star's spin period, and ψ is the angle between the star's spin and $\mathbf{n}_{\rm G}$.

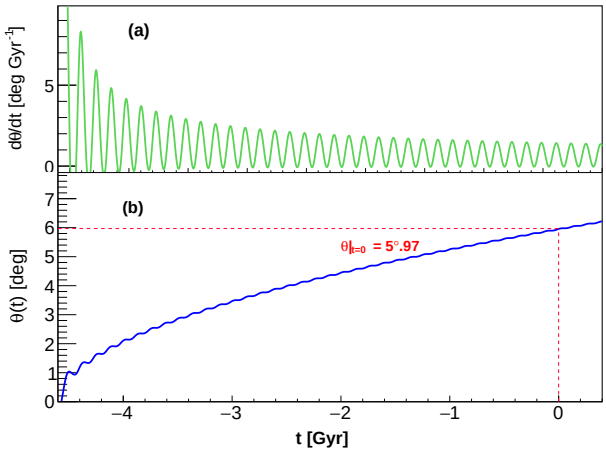

Figure 2 A hypothetical scenario that the observed θ today ($\theta \simeq 5^\circ.97$) was caused purely from a nonzero ξ (here $\xi = 1.12 \times 10^{-6}$). The time derivative of $\theta(t)$, $\mathrm{d}\theta/\mathrm{d}t$ in (a), and $\theta(t)$ in (b) are shown as a function of time from the birth of the Solar System ($t \simeq -4.6$ Gyr) to today ($t = 0$). Oscillation is caused by the Sun's revolving around the Galactic center (~ 20 circles in 4.6 Gyr), while the decreasing amplitude in (a) is due to the decreasing rate of Solar spin [71].

From our understanding of planetary systems, at the birth of the Solar System ~ 4.6 Gyr ago, the angle θ between the Sun's spin and the total angular momentum of the Solar System was likely very small. Afterwards, the Newtonian torque is negligibly weak to change θ significantly. Today's observations reveal a small $\theta \simeq 5.97^\circ$ [69]. Nordtvedt suggested to use the observed θ as an upper limit for ξ-induced precession angle during ~ 4.6 Gyr to constrain ξ in Eq. (14). Detailed studies, taking the Sun's revolving around the Galactic center into account, were carried out recently [62]. Figure 2 illustrates a hypothetical scenario where a nonzero ξ increases θ gradually from 0° to its current value. In contrast to a constant Solar spin rate that was used in Ref. [62], we here adopt the suggestion in Ref. [70] and use the Skumanich law, $P \propto (t - t_0)^{-1/2}$, for the evolution of spin rate [71]. A simple calculation shows that, the adoption of Solar spindown model tightens the limit of $|\xi|$ in Ref. [62] by a factor of two.

More simulations were performed in Ref. [62]. It showed that, by a rough conjecture that θ was less than 10° at the birth of the Solar system, ξ can be limited to [62],

$$|\xi| < 5 \times 10^{-6} \,. \tag{15}$$

This value was the one obtained in Ref. [62] with a constant Solar spin rate. As shown, it improves by a factor of two if the Solar spindown is included.

Anomalous Spin Precession of Solitary Pulsars. For solitary pulsars, analogous to the Sun, local position invariance violation also produces a free precession of the pulsar spin around its Galactic acceleration with the angular frequency in Eq. (14). For millisecond pulsars the effect is greatly enhanced, compared to the Sun, due to the extremely short rotational period P ($\sim 10^{-3}$ s). The rotation period of the Sun is in contrast about one month ($\sim 10^6$ s). Therefore, even with observations over just ten years (compared to the ~ 4.6 Gyr time-scale in case of the Sun), one can tightly constrain ξ [62].

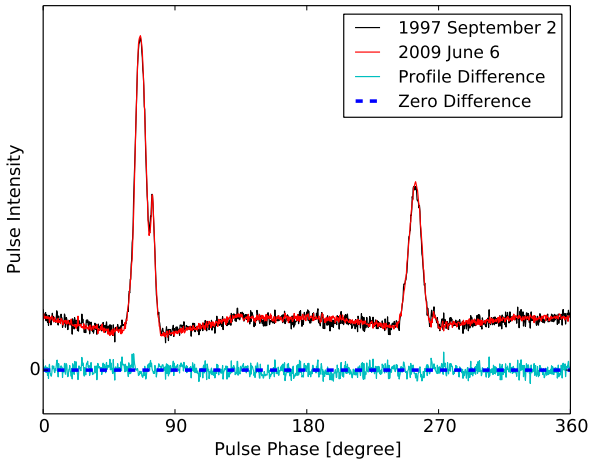

Figure 3 Comparison of two pulse profiles of PSR B1937+21 obtained with the Effelsberg-Berkeley Pulsar Processor at two different epochs — the black one was obtained on 2 September 1997, while the red one was obtained on 6 June 2009. The difference between two profiles is shown in cyan at the bottom. Data of profiles are taken from Ref. [72].

For millisecond pulsars, a hypothetical precession of its spin would cause changes in our line of sight's cutting on its radiation beam. Consequently, we would observe changes in pulse profiles as a function of time. Shao et al. used data from the 100-m Effelsberg radio telescope to study the stability of pulse profiles [72]. A coherent dedispersion backend, the Effelsberg-Berkeley Pulsar Processor, was used, which is the longest-running coherent dedispersion backend dedicated to high-precision pulsar timing in the world, making

the database uniquely suited for the task. Hundreds of pulse profiles of PSRs B1937+21 and J1744−1134, spanning more than ten years, were analyzed homogeneously. Detailed studies showed no pulse profile variations in two pulsars to a high degree [72]. For example, the profile of PSR B1937+21 showed variation in its width at 50% intensity of the main pulse to be less than a few thousandth degrees per year (see Figure 3 for an illustration).

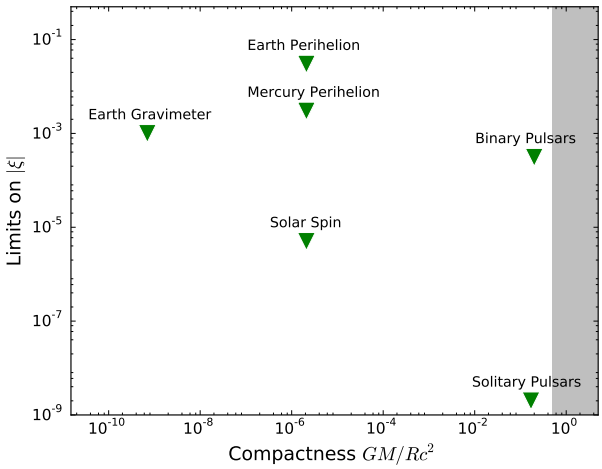

Figure 4 Upper limits on $|\xi|$ from Earth gravimeter [66], Mercury and Earth perihelions [15], Solar spin [62, 64], binary pulsars [63], and solitary pulsars [62], as a function of compactness, $\varepsilon \sim GM/Rc^2$, where M and R are mass and radius, respectively, of the heavier body in the system. Shaded region is the interior of black holes.

The *null detection* of profile variation allowed to limit the precession in Eq. (14) for millisecond pulsars. However, the 3-dimensional spin orientation of the pulsar, which is needed in the calculation, is observationally not fully constrained (although combinations of radio and γ-ray observations can provide partial information, see e.g., Ref. [73]). Therefore, a probabilistic assumption, similar to the case of binary pulsars, was made to account for an unknown angle. With a cone model approximating the radiation pattern [68, 74], PSRs B1937+21 and J1744−1134 give at 95% confidence levels [62]

$$|\xi| < 2.2 \times 10^{-8}\,, \tag{16}$$
$$|\xi| < 1.2 \times 10^{-7}\,, \tag{17}$$

respectively. The probability distribution functions of ξ (see Figure 4 in Ref. [62]) have long tails that result from the probabilistic assumption about the unknown angle. By combining the probability distribution functions of two pulsars, a much tighter limit was obtained [62],

$$|\xi| < 3.9 \times 10^{-9}\,, \tag{18}$$

at 95% confidence level. This is currently the best limit on local position invariance violation in the gravitational interaction [3]. It can also be converted to an upper limit on the spatial anisotropy of the gravitational constant through Eq. (10),

$$\left|\frac{\Delta G}{G}\right|^{\text{anisotropy}} < 4 \times 10^{-16} \quad (95\%\ \text{CL})\,. \tag{19}$$

Figure 4 summarizes the limits on ξ discussed above, as a function of the compactness of the system, $\varepsilon \sim GM/Rc^2$, where M and R are the mass and the radius of the system. In the case of binary systems, the quantities of the heavier body are used. For pulsars with unknown mass and/or radius, canonical values of $M \sim 1.4\,\mathrm{M}_\odot$ and $R \sim 12\,\mathrm{km}$ are assumed. The figure clearly shows that the limit from solitary pulsars [62] not only poses the tightest constraint, but also probes certain strong-field aspects that are not available in experiments with weakly self-gravitating bodies.

4 Local Lorentz Invariance

The possibility to break local Lorentz invariance found great interest in the gravity community recently [3, 12, 13, 21, 47, 48, 75-78]. Theoretically, it is mainly driven by the attempts to quantize the gravitational interaction. Some models from string theory and loop quantum gravity predict a possible breakdown of the Lorentz symmetry with novel dynamics of spacetime [79-81]. As mentioned before, Hořava-Lifshitz gravity tries to construct a power-counting renormalizable, UV complete gravity theory, at the cost of Lorentz symmetry breaking by using different scalings to the temporal and spatial decomposition of spacetime [12, 13]. For these theories, even at low energy scales, the full Lorentz symmetry is not restored. Lorentz symmetry breaking will manifest tiny deviations in our precision experiments, thus it probably provides us with a precious *quantum gravity window* [6, 77]. In addition to the above mentioned theoretical suspicion, experimentally exploring the boundary of fundamentally treasured symmetries is always considered, and historically verified, as one of the best tools in searching for new physics beyond our current understanding [3].

The breakdown of Lorentz invariance can already happen in flat spacetime where the Lorentz symmetry of special relativity is altered. This in turn breaks Einstein's equivalence principle (EEP). However, under the circumstances where EEP is respected (hence the Lorentz symmetry of special relativity is fully preserved), the local Lorentz invariance in gravitational interaction can still be violated [15]. We are interested here in the latter possibility. Experimental phenomena of local Lorentz invariance violation in gravity were explored vastly at different length scales, from laboratory short-range gravity at $\sim \mu$m [82] to the cosmological scale [83]. This review is not intended to cover the whole field, but rather to highlight the contributions from pulsar astronomy to tests of local Lorentz invariance at length scales of the astronomical unit (AU; $1\,\mathrm{AU} \simeq 1.5 \times 10^{11}\,\mathrm{m}$), and with possible strong-gravity effects associated with neutron

stars [19,20,33,34,84-88]. Two popular frameworks with local Lorentz invariance violation in gravity are considered in the following.

4.1 Metric-based framework: PPN

In the field of experimental gravity, the most popular framework is the parametrized post-Newtonian (PPN) formalism, proposed by Kenneth Nordtvedt and Clifford Will in late 1960s and early 1970s [65,89]. The construction of PPN formalism was inspired by the experimental precision of WEP at that time and thence the requirement of a metric theory of gravitation that fulfills the EEP [3]. In metric theories of gravitation, despite the possible existence of long-range gravitational fields (e.g., scalar fields in scalar-tensor theories [90]), matter and all non-gravitational fields only couple to the (physical) metric $g_{\mu\nu}$ [3,15]. For instance, the motion of test particles follows the geodesics of the geometry, described by the symmetric rank-2 metric tensor. Consequently, all test bodies, independent of their composition, fall in the same way, which means that WEP is fulfilled. More generally, metric theories of gravity fulfill the EEP, which is also one of the building blocks for PPN formalism.

In the PPN framework, generic ways of how the metric depends on the energy-momentum content of matters are considered. In the PPN gauge, the dependence of the metric components on the matter content can be found in the classical reviews by Will [3, 15]. Ten PPN parameters control, at the first post-Newtonian order, the couplings between the metric and various matter potentials, including the well-known Newtonian "scalar" potential, and vectorial/tensorial ones. Ten PPN parameters are intelligently organized to describe different aspects of gravitation. For example, the Eddington-Robertson-Schiff parameters, β and γ, describe the nonlinearity in the superposition law of gravity and the amount of space-curvature produced by a unit rest mass, respectively. PPN parameters, α_1, α_2 and α_3 parametrize different effects related to a gravitationally preferred frame, which is to be discussed here (α_3 is in addition related to energy-momentum conservation; see below). From the last forty years, there are quite some remarkable limits from various experiments. In this subsection, to keep the scope of this review controllable, we will focus on the constraints of α_1, α_2, and α_3 from radio pulsars, while interested readers are encouraged to read Refs. [3, 15] for more details.

Orbital polarization of binary pulsars with a preferred frame. We will discuss the "orbital polarization" phenomenon introduced by a nonzero α_1, and the relevant experimental tests from binary pulsars. In the generic framework of PPN formalism, there could be a preferred frame where the gravitational interaction is isotropic. If a system is moving with respect to this rest frame, its "absolute" movement is manifest in the gravitational interactions inside the frame that is attached to the system. Equivalently speaking, the gravitational interaction of an isolated system of masses depends on the movement of the frame. Such a preferred frame could have been formed at a very early stage in the cosmological evolution of the Universe or from local matter distributions. The widely adopted practice is to use the frame where the cosmic microwave background (CMB) is isotropic at first order approximation. We will call it the CMB frame.

We consider the orbital dynamics of a two-body system, using a binary pulsar as a prototype. If a binary pulsar is moving with respect to such a preferred frame with an absolute velocity, $\mathbf{w}$, its orbital dynamics is determined by the post-Newtonian Lagrangian, L, where, in addition to the contributions from Newtonian gravity and general-relativistic corrections, we have extra contributions from α_1 and α_2[4],

$$L_{\alpha_1} = -\alpha_1 \frac{Gm_1m_2}{r}\frac{\mathbf{v}_1^0\cdot\mathbf{v}_2^0}{2c^2}, \quad (20)$$

$$L_{\alpha_2} = \alpha_2 \frac{Gm_1m_2}{r}\frac{\left(\mathbf{v}_1^0\cdot\mathbf{v}_2^0\right)-\left(\mathbf{n}\cdot\mathbf{v}_1^0\right)\left(\mathbf{n}\cdot\mathbf{v}_2^0\right)}{2c^2}, \quad (21)$$

where $\mathbf{v}_i^0$ $(i=1,2)$ is the absolute velocity of body i.

Damour and Esposito-Farèse are the first to study the possibility of local Lorentz invariance violation in PPN formalism within the context of pulsar timing [84]. Because of the tight limit of α_2 from spin evolution of the Sun (see below) at that time [64], they discarded the term proportional to α_2, namely Eq. (21). With the contribution of Eq. (20), Damour and Esposito-Farèse advised a pictorial way to capture the secular influence of α_1 on the dynamics of the quasi-circular orbit. The effect is included in the evolution of the orbital eccentricity vector, $\mathbf{e}\equiv e\mathbf{a}$, where e is the magnitude of the orbital eccentricity and $\mathbf{a}$ is the unit vector pointing from the center of mass of the system to the orbital periastron. The evolution of $\mathbf{e}$ is illustrated in Figure 5 and explained as follows in different gravity theories.

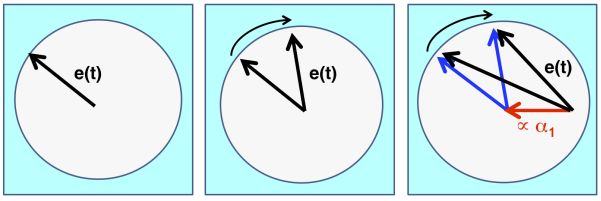

Figure 5 Graphical illustration of the evolution of the eccentricity vector, $\mathbf{e}(t)$, for quasi-circular orbits in (*left*) Newtonian gravity, (*middle*) general relativity, and (*right*) PPN formalism with a nonzero α_1. Black arrows, $\mathbf{e}(t)$, represent the eccentricity vectors in observation.

- In Newtonian gravity, it is well known that the $\propto r^{-2}$ force has the symmetry group of $O(4)$ instead of $O(3)$, therefore, the unit vector $\mathbf{a}$ is a conserved quantity, hence $\mathrm{d}\mathbf{e}/\mathrm{d}t = 0$.

- In GR, Einstein derived the famous periastron advance rate for the Mercury [2]. In the first post-Newtonian

[4] We ignore the contributions from β and γ for the moment, and postpone the contributions from other PPN parameters.

approximation, the (orbital averaged) eccentricity vector $\mathbf{e}(t)$ rotates uniformly as a function of time.

- In addition to GR, if a nonzero α_1 exists, the eccentricity vector $\mathbf{e}(t)$ can be viewed as a vectorial superposition of a forced eccentricity, $\mathbf{e}_{\rm F}$, that is a constant vector in the orbital plane, and a rotating eccentricity, $\mathbf{e}_{\rm R}(t)$, that rotates according to the relativistic precession rate of periastron [84], and is constant in length. The observed eccentricity vector $\mathbf{e}(t) = \mathbf{e}_{\rm F} + \mathbf{e}_{\rm R}(t)$.

In early work, because of the lack of suitable systems and essential observations to perform a direct test of the above dynamics, probabilistic approaches were adopted, analogue to the Damour-Schäfer test described in Section 2 [84, 91]. Later the method was extended to statistically combine multiple systems by taking care of a potential selection effect when simply picking a system with the most favorable parameter combination [92]. In addition, because the 3-dimensional velocity of the binary pulsar systems cannot be fully obtained from radio timing, one has to invoke probabilistic assumptions for the radial velocity of most of the binary systems used in the analyses. Originally, PSRs 0655+64 and 1855+09 were used to obtain the first limit of α_1 in pulsar timing experiment [84]. Later, PSR J2317+1439 was used to update its value [91]. A direct method to measure the influence of α_1 on orbital dynamics was developed in Ref. [93], where a timing formula including Lorentz-violating effects from α_1 and α_2 is constructed for the double pulsar system. However, with 3-year timing data of the Double Pulsar [94], the constraints on α_1 and α_2 are quite weak. Because the orbit of double pulsar is nearly edge-on with respect to its line of sight [94], the timing formula gets simplified. For a generic orbital orientation, it can be rather complicated.

The best constraint on α_1 comes from a new method, based on the observations of small-eccentricity neutron star – white dwarf binaries [86]. It is a direct method that looks for time variation of the eccentricity vector, instead of using the magnitude of the eccentricity as in the aforementioned probabilistic approaches. The problem related to the measurement of 3-dimensional spatial velocity is resolved by using extra information from optical observations of the white dwarf companion. From combined information of radio timing of the pulsar and high-resolution spectroscopy of the white dwarf, the 3-dimensional spatial velocity of the binary can be obtained, therefore, the absolute velocity of the system with respect to the CMB frame is known. In the direct approach, all quantities that enter the differential equations of orbital dynamics are known, except the longitude of ascending node, Ω. We performed extensive simulations to evolve the orbit according to the post-Newtonian dynamics with a nonzero α_1 for all possible values of $\Omega \in [0^\circ, 360^\circ)$, and from simulations to infer what kind of eccentricity variation, in terms of both magnitude and direction, would be consistent with real observations. The α_1 values that result in eccentricity variations compatible with real observational data are kept. From the distribution of α_1 for every Ω, we were able to obtain an upper limit of α_1 as a function of Ω. From these results, we picked the most conservative one as our final limit, thus thoroughly avoided the probabilistic assumption of Ref. [86].

In the approach outlined above, we obtained upper limits from PSRs J1012+5307 and J1738+0333. Both systems have multiwavelength observations. In particular the optical observations of their white dwarf companions are very useful in giving 3 dimensional velocity and component masses in a way that is independent to the underlying gravity theory [20]. Among other factors that affect the test, the orbit of PSR J1738+0333 has a better relative geometrical orientation with respect to the absolute velocity of the system in the CMB frame. Therefore, a better limit was achieved in that system. At 95% confidence level, the analysis of PSR J1738+0333 gives,

$$\alpha_1 = -0.4^{+3.7}_{-3.1} \times 10^{-5} \,. \tag{22}$$

It is the currently best limit of the PPN parameter α_1 [3]. If a similar mechanism to the cosmological attractor in scalar-tensor theories [95] exists for the PPN parameter α_1 (as for the Eddington-Robertson-Schiff parameters β and γ), the new limit at the level of $O(10^{-5})$ in Eq. (22) has started to enter cosmologically interesting parameter space.

Orbital precession of binary pulsars. As stated above, Damour and Esposito-Farèse initiated the program of using pulsar timing to probe the local Lorentz invariance in the gravity sector [84]. We followed their work and derived the joint influence of α_1 and α_2 on the orbital dynamics of an eccentric binary [86]. It is interesting to discover that, for small-eccentricity binaries with $e \ll 1$, the effects of α_1 and α_2 on orbital dynamics decouple. While the α_1 parameter tries to polarize the orbit, its effect is inside the orbit; in contrast, the α_2 parameter has an effect "perpendicular" to the orbit in the sense that it tries to rotate the orbit along the direction of the absolute velocity of the binary, $\mathbf{w}$. The precession rate is [86],

$$\Omega^{\rm orbit}_{\alpha_2} = -\alpha_2 \frac{\pi}{P_b} \left(\frac{w}{c}\right)^2 \cos\psi_{\rm orbit} \,, \tag{23}$$

where P_b is the orbital period and $\psi_{\rm orbit}$ is the angle between orbital angular momentum and the direction of $\mathbf{w}$. In pulsar timing, such a precession will change the angle between our line of sight and the orbital plane, hence change the projected semimajor axis of the pulsar orbit, which is an observable in timing experiments. The upper limits of the change in the projected semimajor axis can be used to constrain such an α_2-induced precession. After carefully subtracting other potential contributions to the change of projected semimajor axis, we were able to reach a limit of,

$$|\alpha_2| < 1.8 \times 10^{-4} \,, \tag{24}$$

from the combination of PSRs J1012+5307 and J1738+0333 at 95% confidence level [86]. In obtaining the above quoted limit, a probabilistic assumption about Ω has to be made, and we also made an assumption of a weak compactness-dependence of α_2 for the two pulsars used in the test.

Spin precession of solitary pulsars. The limit of α_2 obtained from binary pulsars is much weaker than the limit from the spin evolution of the Sun, that is at the level of $O(10^{-7})$ [64]. As for the ξ parameter discussed above, Nordtvedt calculated the effect of α_2 on a rotating massive body with internal equilibrium, and found that the spin direction of such a body would precess around the direction of its absolute movement at a rate,

$$\Omega^{\rm spin}_{\alpha_2} = -\alpha_2 \frac{\pi}{P}\left(\frac{w}{c}\right)^2 \cos\psi_{\rm spin}\,, \tag{25}$$

where P is the rotation period of the body and $\psi_{\rm spin}$ is the angle between spin direction and $\mathbf{w}$. This precession formula is very similar to the orbital precession rate in Eq. (23) with replacements of $P_b \to P$ and $\psi_{\rm orbit} \to \psi_{\rm spin}$. It is because that for a uniformly rotating extended body, its constitution particles can be viewed as pairs in orbit with period P, and the orbits of these pairs all precess with an angular velocity $\Omega^{\rm orbit}_{\alpha_2}$, therefore the extended body as a whole precesses with $\Omega^{\rm spin}_{\alpha_2}$. The disproportional gravitational forces in above analogy are compensated by the forces from the internal pressure.

Nordtvedt assumed that the spin of the Sun was in parallel with the total angular momentum of the Solar system when the Solar system was formed about five billion years ago, and used the currently observed misalignment angle $\sim 6^\circ$ as an upper limit to constrain the possible precession of the Solar spin introduced by a nonzero α_2 [64]. This approach is very effective due to a long time baseline of precession, about five billion years, therefore, a very tight limit of α_2 at the level of $O(10^{-7})$ was achieved.

Nordtvedt pointed out briefly that observations of pulsars can also be used to constrain α_2 [64] if possible observational quantities could be firmly identified. PSRs B1937+21 (the first discovered millisecond pulsar) and B0531+21 (the Crab pulsar) were used as potential examples in his discussion. Following this suggestion, Shao et al. [72] were the first to firmly connect pulsar observations to the theoretical prediction of the spin precession introduced by a nonzero α_2. If such a precession exists for solitary pulsars, it will introduce changes in our line of sight cutting the emission region of pulsars' magnetosphere. Therefore, we are supposed to see drifts in pulse profiles as a function of time. As mentioned before, pulse-profile observations of two millisecond pulsars, PSRs B1937+21 and J1744−1134, conducted at the Effelsberg radio telescope, were analyzed homogeneously to obtain information about the possibility of such a drift. From data collected with the Effelsberg-Berkeley Pulsar Processor (EBPP) backend, covering more than ten years, no detectable change in profiles is identified. Quantitative limits on the change of widths, change of peak separations, and change of peak intensity ratios, of pulse profiles, were obtained (see Figure 4 and Table 1 in Ref. [72]). With a reasonable geometrical model for the pulsar emission, the observed (non-)change in pulse profile is linked to the (non-)precession of the pulsar spin. Analogous to the limit on ξ described in Section 3, new limits for α_2 were inferred from the absence of precession given by Eq. (25).

In performing the test, we need the full geometrical information about the spin direction of pulsars, and the relative movements of pulsars with respect to a preferred frame, which, unfortunately, are not fully attainable. Instead of the 3 dimensional velocity, we can only obtain its 2 dimensional projection on the sky plane, namely the proper motion. However, with the knowledge of the Galactic potential of the Milky Way, we can get a reasonable range for the velocity along the line of sight (the unknown radial velocity), by assuming that the pulsar is gravitationally bound to the Galaxy. Our limit of α_2 is not very sensitive to the radial velocity in that range. For two angles that describe the spin direction, we can infer one of them, the polar angle, with the help of γ-ray observations from the Fermi satellite. The other angle, the azimuthal one, is assumed to be uniform in the range of $[0^\circ, 360^\circ)$ probabilistically. After taking all experimental uncertainties and the probabilistic assumption into account, we obtained at 95% confidence level,

$$|\alpha_2| < 1.6 \times 10^{-9}\,, \tag{26}$$

from the combination of PSRs B1937+21 and J1744−1134 [72].

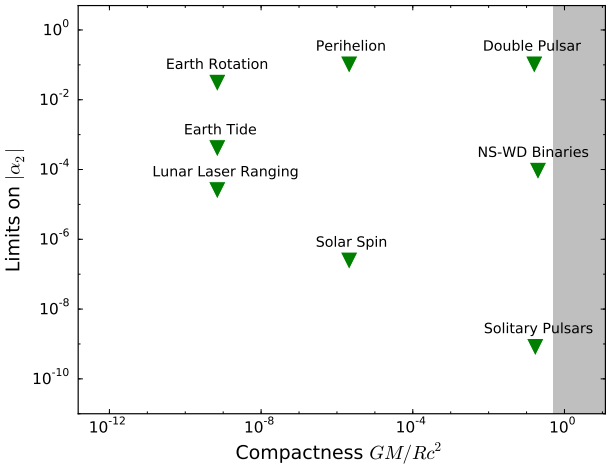

Figure 6 Upper limits on $|\alpha_2|$ from Earth rotation [15], Earth tides [15,66], planetary perihelion [15], LLR [96], Double Pulsar (based on data up to 2006) [93], Solar spin [64], neutron star – white dwarf binaries [86], and solitary pulsars [62], as a function of compactness, GM/Rc^2, where M and R are mass and radius, respectively, of the heavier body in the system. Shaded region is the interior of black holes.

In Figure 6 we plot the limits of α_2 from various observations as a function of the compactness of the system [3, 15]. The limit from pulse-profile observations of pulsars not only constitutes the currently best limit of α_2 [3], but also probes a parameter region that strong gravitational fields are present.

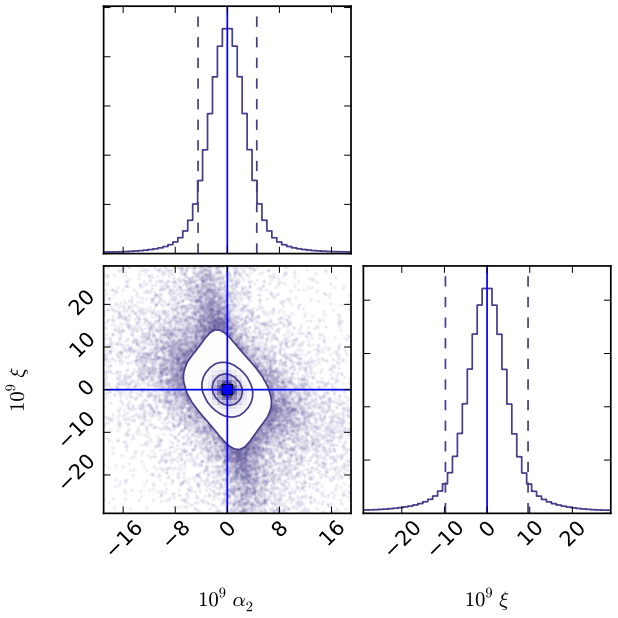

Figure 7 Distributions of (α_2, ξ) pairs whose effects on the spin precession of solitary pulsars, PSR B1937+21 and J1744−1134, are compatible with observations. The values of α_2 and ξ in GR are marked in blue. The marginalized probability densities of two parameters are shown as histograms where dash lines enclose the 90% confidence region.

As discussed in detail in Section 3, the PPN parameter ξ, that describes the local position invariance violation, introduces a similar precession of the spin of solitary pulsars, and were constrained by the same set of observations of PSRs B1937+21 and J1744−1134 independently [62]. The precessions introduced by α_2 and ξ are around different directions ($\mathbf{w}$ and $\mathbf{n}_{\rm G}$, respectively). Possible correlation between α_2 and ξ is expected. We performed new simulations that include the possibility that both ξ and α_2 can be nonzero. The result on the change in pulse widths from simulations with randomly generated (α_2, ξ) pairs is compared with pulse-profile observations in Ref. [72]. In Figure 7 we plot the (α_2, ξ) pairs in our simulations that are compatible with the observational constraints. The quantitative limits on the changes of pulse profiles of PSRs B1937+21 and J1744−1134 are used, and an assumption of a uniform distribution of η in $[0°, 360°)$ is made. As we can see from the figure, because we have two observational constraints to be satisfied from two pulsars, the degeneracy between α_2 and ξ is broken to some degree. The consideration of simultaneously nonzero values for α_2 and ξ does not degrade too much the previous limits, based on only one nonvanishing PPN parameter. The change is only a factor of a few. We also performed mock simulations to check further improvement of these limits by including a third hypothetical pulsar with the same level of quality in pulse-profile observation. It can improve our joint limits to the level when only one parameter is considered nonzero. This improvement largely comes from the suppression of long tails in the posterior distributions (as discussed in detail in Ref. [86]).

Again, if a similar mechanism to the cosmological attractor in scalar-tensor theories [95] exists for the PPN parameter α_2, the new limit from pulsar pulse profiles at the level of $O(10^{-9})$, namely Eq. (26), has definitely entered into a region that can be used to constrain the attractor mechanism. The limit is also interesting for phenomena in cosmology with Lorentz-violating gravity [83].

Orbital polarization of binary pulsars with self acceleration. The α_3 parameter has double effects as it violates the local Lorentz invariance and the energy-momentum conservation law in gravity [3]. The existence of a nonvanishing α_3 could introduce interesting phenomena with anomalous planetary perihelion precession [65], anomalous time derivative of pulsars' spin [15], and polarization of binary orbits [97]. In pulsar timing experiments, the best constraint of α_3 comes from its effects on orbital dynamics of binary pulsars [33, 34, 92, 97, 98].

The PPN parameter α_3 breaks the conservation of energy-momentum, introducing a self acceleration on spinning bodies with self-gravity [15, 97],

$$\mathbf{a}_{\alpha_3} = -\frac{1}{3}\frac{E^{\rm grav}}{Mc^2}\mathbf{v}^0 \times \mathbf{\Omega}\,, \tag{27}$$

where $\mathbf{v}^0$ is the absolute velocity, $\mathbf{\Omega}$ is the spinning angular velocity, and $E^{\rm grav}$ is the gravitational self-energy. It is easily seen that, i) the more compact the body (hence a larger $|E^{\rm grav}/Mc^2|$), the larger the effect of α_3; ii) the more rapidly spinning the body, the larger the effect of α_3. Millisecond pulsars represent best laboratories so far for testing this PPN parameter.

Both spin derivative of solitary pulsars and orbital polarization of binary pulsars were used to constrain α_3. Here we will emphasize the latter, for it gave a significantly better limit. The effect of α_3 on the binary orbit is very similar to the effects of GWEP violation in Section 2 and α_1 that we discussed before. It introduces a "gravitational Stark effect" that polarizes the orbital eccentricity vector for quasi-circular neutron star – white dwarf orbits with the pulsar spin perpendicular to the orbital plane [97]. Similar to the case shown in Figure 5, a nonzero α_3 makes the observed eccentricity vector a superposition of two vectors, like in Figure 5, namely, a rotating vector, precessing with the rate of the relativistic periastron advance, and a fixed vector that is inside the orbital plane with a direction perpendicular to both the pulsar spin and the system's absolute velocity [97]. The assumption that the spin of the pulsar is aligned with the orbital angular momentum is well justified for recycled millisecond pulsars. In contrast to α_1, the extra contribution with a nonzero α_3 is nonconservative, in the sense that it violates momentum conservation. It is a self-acceleration effect.

With probabilistic assumptions about the relative orientation of the pulsar orbit with respect to the absolute velocity $\mathbf{w}$, and the relative angle between the rotating eccentricity

and the fixed eccentricity, Bell and Damour obtained a limit of $|\alpha_3| < 2.2 \times 10^{-20}$ at 90% confidence level. Later, it was updated several times with new observations [33, 34, 92] and more sophisticated statistical treatments, leading to $|\alpha_3| < 5.5 \times 10^{-20}$ at 95% confidence level [34]. The most recent limit comes from PSR J1713+0747, and gives $|\alpha_3| < 2\times10^{-20}$ at 95% confidence level [98]. This remarkable limit is even a million times better than the limits on the violation of WEP [3]. One needs to keep in mind, however, that this last limit is based on the Damour-Schäfer test applied to a single system, and should therefore be taken with some caution, as outlined previously. On the other hand, in the meantime, with new constraints on a temporal variation in the eccentricity, PSR J1713+0747 is very well suited for a direct test of α_3 (Zhu et al., in prep.).

4.2 Action-based framework: SME

Two pillars of modern theoretical physics, *i.e.*, the standard model of particles and the general relativity of gravitation, can be elegantly expressed in the language of field theory, where the action, $S \equiv \int \mathcal{L} \mathrm{d}^n x$, with the Lagrangian density $\mathcal{L}$ and the spacetime dimension n (we fix $n = 4$ hereafter), plays a prominent role. Classically, the dynamics of physics is obtained with the principle of least action, that requires a vanishing change in the action, $\delta S = 0$, with independent variational changes in its dynamical field variables. It results in an extremum of the action integral and picks out the extremal paths.[5] From a field-theoretical viewpoint, the action, or equivalently the Lagrangian density, encapsulates the physical dynamics.

Historically, shortly after Albert Einstein established the field equations of gravitation [1], David Hilbert proposed its corresponding action formulation [99] starting with the *Einstein-Hilbert action* [17],

$$S_{\mathrm{EH}} = \frac{1}{16\pi G} \int \sqrt{-g}(R - 2\Lambda)\mathrm{d}^4 x \,, \tag{28}$$

where R is the Ricci scalar and Λ is the cosmological constant (we set $\Lambda = 0$ for localized systems). To go beyond Einstein's GR, new gravitational degrees are added to the above action with suitable forms, like the scalar degree in scalar-tensor theories [26-28, 100, 101] mentioned in Section 2.

Since GR performed extraordinarily well in a variety of experiments, only tiny deviations from GR are allowed in the regimes that have been probed, if assuming the absence of nonperturbative strong-field dynamics. Therefore, effective field theories with effective degrees that come from deeper fundamental (unknown) theory fit the context. Standard model extension (SME) is constructed as a convenient experimentally working framework to probe all possible Lorentz-violating deviations in the spirit of effective field theories [79, 80, 102, 103]. In the limit of Riemannian spacetime and the pure-gravity sector with Lorentz-violating operators of mass dimension four or less (the so-called *minimal* SME), the only possible Lagrangian with gauge invariance, energy-momentum conservation, and Lorentz-covariant dynamics, is [21, 76]

$$\begin{aligned} S \;=\; & \frac{1}{16\pi G} \int \Big[\sqrt{-g}\Big(R - 2\Lambda - uR + s^{\mu\nu} R^{\mathrm{T}}_{\mu\nu} + t^{\kappa\lambda\mu\nu} C_{\kappa\lambda\mu\nu}\Big) \\ & - V(\cdot)\Big] \mathrm{d}^4 x \,, \end{aligned} \tag{29}$$

where $R^{\mathrm{T}}_{\mu\nu} \equiv R_{\mu\nu} - g_{\mu\nu}R/4$ is the traceless Ricci tensor and $C_{\kappa\lambda\mu\nu}$ is the Weyl conformal tensor; u, $s^{\mu\nu}$, and $t^{\kappa\lambda\mu\nu}$ are additional dynamical fields, and $V(\cdot)$ collectively denotes their (unspecified) potentials.

In the context of SME, to be fully consistent with the Riemannian geometric setup, the fields u, $s^{\mu\nu}$, and $t^{\kappa\lambda\mu\nu}$ seek their cosmological values with minimization of $V(\cdot)$ through the mechanism of spontaneous symmetry breaking [21]. These fields acquire background values $\bar{u}$, $\bar{s}^{\mu\nu}$, and $\bar{t}^{\kappa\lambda\mu\nu}$, respectively. Contrast to the traditional Higgs mechanism [104, 105], the symmetry breaking here involves tensor degrees, so the local Lorentz symmetry of spacetime is consequently broken if the vacuum expectation values of these tensor fields are nonzero. After adopting several plausible assumptions and taking care of fluctuations around the vacuum expectation values, including massless Nambu-Goldstone modes, Bailey and Kostelecký were able to explore the experimental phenomena of Eq. (29) at the leading post-Newtonian order [76]. At the leading order, $\bar{t}^{\kappa\lambda\mu\nu}$ does not show up [106], and $\bar{u}$ can be absorbed into a redefinition of the gravitational constant G. Therefore, we are left with nine degrees of freedom with the symmetric and traceless tensor, $\bar{s}^{\mu\nu}$, which is the primary object we are to deal with in the following text.

In an asymptotically flat coordinate frame, $\bar{s}^{\mu\nu}$ is simply a constant dimensionless matrix. Between asymptotically flat frames chosen by experimenters, $\bar{s}^{\mu\nu}$ transforms according to canonical Lorentz transformation laws.[6] To facilitate comparisons between different experiments, $\bar{s}^{\mu\nu}$ are often reported in the asymptotically inertial frame, $(\partial_T, \partial_X, \partial_Y, \partial_Z)$, that is comoving with the rest frame of the Solar System and that coincides with the canonical Sun-centered frame [76]. Comparisons of SME with the PPN framework and Nordtvedt's anisotropically parametrized post-Newtonian model [108] can be found in Ref. [76].

[5] Quantum mechanically, in the language of path integral, all paths are equal-probabilistic, but paths that are not extremal mutually cancel out vastly because of lack of accordance in their phases, and in the classical limit where the Planck constant $\hbar \to 0$, only the extremum contributes.

[6] See Refs. [76, 107] for distinctions between particle Lorentz invariance and observer Lorentz invariance. In the context of SME, particle Lorentz invariance is broken, while observer Lorentz invariance preserves.

[7] Recently, there are some experimental exploration for operators with mass dimension higher than four in the pure-gravity sector of SME (the so-called *non-minimal* SME). It belongs to the short-range gravity regime, and is beyond the scope of current paper. Interested readers are pointed to Refs. [82, 109, 110]. Moreover, phenomena with Lorentz-violating matter-gravity couplings can be found in Refs. [78, 111-113].

Experimental tests of the pure-gravity sector of SME include perihelion shift, time-delay effect, lunar and satellite laser ranging, gravimeter, torsion pendulum, gyroscope, binary pulsars, and so on [76].[7] We will review results from LLR [114], atom interferometry [115, 116], Gravity Probe B [117], planetary orbital dynamics [118], and millisecond radio pulsars [87, 119, 120]. These results are collected by the updating arXiv version of *Data tables for Lorentz and CPT violation* [121].

Lunar Laser Ranging. Lunar laser ranging experiment has been ongoing since the Apollo mission put retroreflectors on the Moon surface in 1969. It measures the Earth-Moon separation by timing the round-trip flight of light between ranging stations on the Earth surface and retroreflectors on the Moon surface [122]. The precision has now reached $\delta x/d_{\oplus\leftmoon} \sim$ (a few millimeters)/(384400 km) $\sim$ a few parts in 10^{12}, where δx is the timing uncertainty in distance and $d_{\oplus\leftmoon}$ is the average Earth-Moon separation.

Local Lorentz invariance violation would manifest as oscillatory perturbations to the lunar orbit at specific frequencies [76, 114],

$$\delta d^{\rm SME}_{\oplus\leftmoon}(t) = \sum_n \left[A_n \cos(\omega_n t + \phi_n) + B_n \sin(\omega_n t + \phi_n)\right] . \quad (30)$$

The dominant perturbations occur at four frequencies, $\omega_{\leftmoon}$, $2\omega_{\leftmoon}$, $2\omega_{\leftmoon} - \omega'_{\leftmoon}$, and $\omega_\oplus$, where $\omega_{\leftmoon}$ is the sidereal lunar orbital frequency, $\omega'_{\leftmoon}$ is the anomalistic lunar orbital frequency, and $\omega_\oplus$ is the sidereal Earth orbital frequency. The amplitudes, A_n and B_n, and phases, ϕ_n, were calculated by Bailey and Kostelecký [76]. The dominant contributions to $\delta d^{\rm SME}_{\oplus\leftmoon}(t)$ are controlled by six linear combinations of $\bar{s}^{\mu\nu}$ in A_n and B_n.

Battat et al. used 14401 normal points taken at the McDonald Laser-Ranging Station in Texas and the Observatoire de la Côte d'Azur Station in Grass, spanning from 1969 to 2003, to look for possible hints of nonzero SME parameters [114]. They found six linear combinations of $\bar{s}^{\mu\nu}$ consistent with zero and constrained them to the level of 10^{-6} to 10^{-11} (see Table 3 in Ref. [114]).

Atom Interferometry. A relatively recent setup for precision tests of gravity uses atom interferometry, where a freely falling frame is realized with neutral atoms to an outstanding accuracy [123, 124]. The quantum phase of cold atoms is influenced by the local gravitational acceleration $\mathbf{g}$. The phase difference in two interferometric paths can be measured with a great precision when the paths are recombined at a final beam splitter [115, 116].

With a hypothetical violation in local Lorentz invariance, the gravitational acceleration develops modulations due to the rotation of the Earth and the revolving of the Earth around the Sun,

$$\left[\frac{\delta g(t)}{g_0}\right]^{\rm SME} = \sum_m \left[C_m \cos(\omega_m t + \psi_m) + D_m \sin(\omega_m t + \psi_m)\right] . \quad (31)$$

The dominant contributions occur at frequencies $\Omega_\oplus$, $2\Omega_\oplus$, $\Omega_\oplus \pm \omega_\oplus$, and $2\Omega_\oplus \pm \omega_\oplus$, where $\Omega_\oplus \simeq 2\pi/(23.93\ \text{hr})$ is the rotation frequency of the Earth. The amplitudes, C_n and D_n, and phases, ψ_n, can be found in Refs. [76, 115, 116].

Müller et al. [115] and Chung et al. [116] used a vertical Mach-Zehnder atom interferometer with a resolution up to $8\times10^{-9} g/\sqrt{\text{Hz}}$. They obtained limits on seven linear combinations of $\bar{s}^{\mu\nu}$ with the SME parameters from the Lorentz-violating electromagnetic sector, $\tilde{\kappa}_{e^-}$ and $\tilde{\kappa}_{o^+}$ [102, 103]. These limits are remarkable because they probe gravitational effects at the interface of the quantum world. After assuming vanishingly smallness of $\tilde{\kappa}_{e^-}$ and $\tilde{\kappa}_{o^+}$ [121], these limits were combined with that from LLR [114]. This helps in breaking some degeneracy of parameters, and results in tight constraints on eight components of $\bar{s}^{\mu\nu}$, where one roughly has $|\bar{s}^{\rm TK}| \lesssim 10^{-6}$–$10^{-7}$ and $|\bar{s}^{\rm JK}| \lesssim 10^{-9}$ with $J, K \in \{X, Y, Z\}$; see the third column of Table 1 for numbers.

Gravity Probe B. With precision measurements of LLR and atom interferometry, eight components of $\bar{s}^{\mu\nu}$ have been limited, leaving only the time-time component, $\bar{s}^{\rm TT}$, unconstrained. This component does not enter the orbital dynamics of the Moon nor the phase evolution of cold atoms, hence cannot be studied with these experiments [76]. Gravity Probe B is a gyroscope experiment in orbit around the Earth, that monitors the spin dynamics of four cryogenic gyroscopes onboard, relative to a remote guiding star. The analysis revealed a geodetic-precessing drift and a frame-dragging drift at precision of 0.3% and 19%, respectively, in agreement with GR [125, 126].

A hypothetical existence of Lorentz violation would modify the orbital dynamics of the satellite and the spin-orbit dynamics of gyroscopes. Most notably, the $\bar{s}^{\rm TT}$ component enters the equations of geodetic precession and frame dragging, hence can be studied with Gravity Probe B [76]. The precession rate of gyroscopes onboard Gravity Probe B is,

$$\mathbf{\Omega}_{\rm GPB} = \mathbf{\Omega}^{\rm GR} + \mathbf{\Omega}^{\rm SME} , \quad (32)$$

composing of the conventional general-relativistic contribution, $\mathbf{\Omega}^{\rm GR}$, and an extra contribution from SME Lorentz-violating coefficients, $\mathbf{\Omega}^{\rm SME}$ (see Eqs. (154–156) in Ref. [76] for expressions). Bailey et al. [117] analyzed the effects in detail and obtained the first constraint on the time-time component, $|\bar{s}^{\rm TT}| < 3.8\times10^{-3}$, at 68% confidence level, which was used to break all degeneracies of previous results.

Pulsar Timing. As in the case of LLR, a nonzero $\bar{s}^{\mu\nu}$ background field would modify the orbital dynamics of two massive bodies. For binary pulsars, because that the technique of pulsar timing has the ability to precisely map the (projected) relativistic pulsar trajectory around the common center of the binary motion, the modification would manifest itself in the arrival times of pulse signals. If the modification is significantly larger than the uncertainty of arrival times, one would see significant timing residuals after fitting a canonical timing model based on GR to the dataset [127, 128].

Table 1 Observational constraints on the Lorentz-violating $\bar{s}^{\mu\nu}$ components in the pure-gravity sector of SME [76] at 68% confidence levels, from the combined limits of LLR and atom interferometry [116], Gravity Probe B [117], and pulsar timing [87, 120]. Two limits on $\bar{s}^{\rm TT}$ from pulsar timing correspond to the cases with and without the assumption that the isotropic CMB frame is the preferred frame [120]. See also Ref. [118] for a set of recent constraints from planetary orbital dynamics.

$\bar{s}^{\mu\nu}$ components	Pulsar timing	Other experiments
$\lvert\bar{s}^{\rm TT}\rvert$	$< 8\times10^{-6}$ or $< 1.4\times10^{-4}$ [120]	$< 3.8\times10^{-3}$ [117]
$\bar{s}^{\rm TX}$	$(-5.2,\ 5.3)\times10^{-9}$ [87]	$(-5.7,\ 6.7)\times10^{-7}$ [116]
$\bar{s}^{\rm TY}$	$(-7.5,\ 8.5)\times10^{-9}$ [87]	$(-1.2,\ 1.4)\times10^{-6}$ [116]
$\bar{s}^{\rm TZ}$	$(-5.9,\ 5.8)\times10^{-9}$ [87]	$(-4.2,\ 3.4)\times10^{-6}$ [116]
$\bar{s}^{\rm XY}$	$(-3.5,\ 3.6)\times10^{-11}$ [87]	$(-2.1,\ 0.9)\times10^{-9}$ [116]
$\bar{s}^{\rm XZ}$	$(-2.0,\ 2.0)\times10^{-11}$ [87]	$(-4.1,\ -1.3)\times10^{-9}$ [116]
$\bar{s}^{\rm YZ}$	$(-3.3,\ 3.3)\times10^{-11}$ [87]	$(-0.8,\ 2.0)\times10^{-9}$ [116]
$\bar{s}^{\rm XX}-\bar{s}^{\rm YY}$	$(-9.7,\ 10.1)\times10^{-11}$ [87]	$(-2.8,\ 0.4)\times10^{-9}$ [116]
$\bar{s}^{\rm XX}+\bar{s}^{\rm YY}-2\bar{s}^{\rm ZZ}$	$(-12.3,\ 12.2)\times10^{-11}$ [87]	$(-3.6,\ 4.0)\times10^{-8}$ [116]

In the pure-gravity sector of SME, Lorentz invariance violation causes secular changes in orbital elements after averaging over one orbital period [76],

$$\delta\left\langle\frac{{\rm d}\omega}{{\rm d}t}\right\rangle = f_{\dot\omega}^{\rm SME}(P_b,e,i,\Omega,\omega,m_1,m_2;\bar{s}^{\mu\nu}), \quad (33)$$

$$\left\langle\frac{{\rm d}e}{{\rm d}t}\right\rangle = f_{\dot e}^{\rm SME}(P_b,e,i,\Omega,\omega,m_1,m_2;\bar{s}^{\mu\nu}), \quad (34)$$

$$\left\langle\frac{{\rm d}x}{{\rm d}t}\right\rangle = f_{\dot x}^{\rm SME}(P_b,e,i,\Omega,\omega,m_1,m_2;\bar{s}^{\mu\nu}), \quad (35)$$

where $\delta\langle{\rm d}\omega/{\rm d}t\rangle$ is the difference in periastron advance rate with respect to GR, while the contributions from GR to $\langle{\rm d}e/{\rm d}t\rangle$ and $\langle{\rm d}x/{\rm d}t\rangle$ are too small compared with current timing precision [68]. Functions $f_{\dot\omega}^{\rm SME}(\cdots;\cdot)$, $f_{\dot e}^{\rm SME}(\cdots;\cdot)$, and $f_{\dot x}^{\rm SME}(\cdots;\cdot)$ are homogeneous linear forms of $\bar{s}^{\mu\nu}$, and their explicit expressions can be found in Refs. [76, 87, 120]. It is important to note that these functions depend on the projected $\bar{s}^{\mu\nu}$ onto the coordinate system defined by the orbit (see Figure 2 in Ref. [87] for the definition of the coordinate system). The projected $\bar{s}^{\mu\nu}$ can be related to its values in the standard frame of SME through angles $(\alpha,\ \delta)$ and $(i,\ \Omega,\ \omega)$. The rotation matrices of transformation were given explicitly in the supplemental material of Ref. [87] and in Eqs. (19–24) of Ref. [120]. While the underlying $\bar{s}^{\mu\nu}$ field is the same for all binary pulsars, because of different sky locations, characterized by $(\alpha,\ \delta)$, different orbital orientations, characterized by $(i,\ \Omega,\ \omega)$, different orbital characteristics (e.g., orbital period, P_b, orbital eccentricity, e, and so on), the projections are different for different binary pulsars. Therefore, a variety of binary pulsars probe a variety of linear combinations of $\bar{s}^{\mu\nu}$. In the area of pulsar astronomy, the advanced radio telescopes have provided us with dozens of well-timed millisecond binary pulsars (especially within the programs of pulsar timing array [129-132]). It becomes possible to use an array of pulsars to constrain different linear combinations of $\bar{s}^{\mu\nu}$, and finally put all together to break all degeneracy of underlying degrees of freedom with negligible mutual correlation.

However, there are some subtleties related to observational characteristics of binary pulsars [87]:

1. Concerning Eqs. (34–35), usually, $\dot e$ and $\dot x$ are not reported in literature. Conservative surrogates of their values used the observed uncertainties of e and x, by assuming that the observed uncertainties are purely generated from the Lorentz-violating linear-in-time evolution. If there are other contributions to these quantities, the uncertainties are likely to be larger.

2. Because in most binary pulsars, the determination of component masses heavily rely on the measured value of $\dot\omega$. Therefore, to avoid improper cyclic usage, the $\dot\omega$ measurement must not be used in Eq. (33) to test local Lorentz invariance violation, unless the masses can be determined from other observations without using $\dot\omega$. In the sample pulsars of Ref. [87], three white dwarf – neutron star binaries have double-line observations with radio timing on the pulsars and optical spectroscopy on the white dwarfs. The masses of these binaries were determined accurately with the mass ratio from orbital-phase-resolved radio and optical data, and well-tested white dwarf atmosphere models [38, 42, 43]. For consistency, the test in Eq. (33) were performed only for these three binaries.

3. A large $\dot\omega$ can render the secular changes nonlinear in Eqs. (33–35) [93]. Fortunately, the linear-in-time approximation is plausible with the binary samples in Ref. [87] at current stage. Otherwise, more proper timing models are needed; see Ref. [93] for example.

4. To precisely project $\bar{s}^{\mu\nu}$ on the binary orbital frame, one has to account for the boost between the pulsar frame

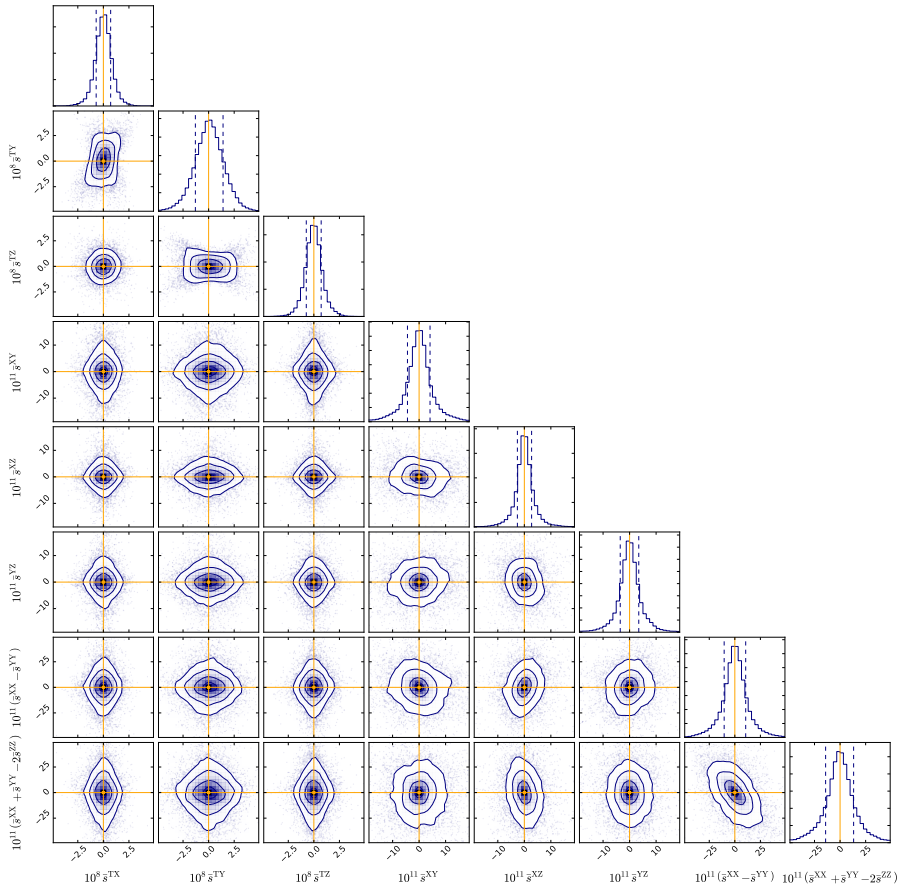

Figure 8 Components of $\bar{s}^{\mu\nu}$ that pass all the tests in the simulation. Their marginalized probability densities are depicted as histograms where dash lines enclose the 68% confidence level. Values of $\bar{s}^{\mu\nu}$ in GR are shown in orange. Data are taken from Ref. [87].

and the frame of the Solar System. However, the 3-dimensional bulky velocity of binaries, $\mathbf{v}^{\rm binary}$, is not always observationally known. From our understanding of binary evolution, the velocity is usually small, $|\mathbf{v}^{\rm binary}| \sim 10^2$ km s^{-1}, compared with the light speed, $c = 3.0 \times 10^5$ km s^{-1}. So at the first-order approximation, the boost effect can be neglected [87]. More on how to wisely use this boost to probe the $\bar{s}^{\rm TT}$ component will be discussed later [120].

5. To fully determine the projection of $\bar{s}^{\mu\nu}$ mentioned before, one has to know the absolute orientation of binary orbits, characterized by (i, Ω, ω), wherein the longitude of ascending node, Ω, is not observationally available for most binary pulsars. Therefore, a probabilistic assumption of Ω was made.

In addition to the modifications in the orbital dynamics of binary pulsars, Eqs. (33–35), a nonzero $\bar{s}^{\mu\nu}$ field would also cause a free precession of the spin of a solitary pulsar [87] at a drift rate,

$$\Omega_k^{\rm SME} = \sum_j \frac{\pi}{P} \bar{s}^{jk} \hat{S}^j \,, \tag{36}$$

where P is the spin period, and $\hat{\mathbf{S}}$ is a unit vector pointing in the direction of the pulsar spin. Again, the $\bar{s}^{\mu\nu}$ field is projected in the frame established by the pulsar system. Such a spin precession would change our line-of-sight cut on the pulsar radiation zone, consequently resulting in changes in the pulse profile as a function of time. It is similar to the case of a nonzero PPN α_2. Null observation of such changes can be used to constrain SME parameters [72] (see Figure 3 for an illustration on the stability of pulse profiles for millisecond pulsars). The azimuthal angle of the pulsar spin is in general not observable, therefore a similar probabilistic consideration as for the Ω in binary pulsars was carried out [87].

Combining all concerns above for binary pulsars and solitary pulsars, Monte Carlo simulations were set up to perform simultaneously twenty-seven tests from thirteen pulsar systems. Because in total there are eight degrees of freedom entering the orbital dynamics of binary pulsars and spin precession of solitary pulsars, twenty-seven tests have overconstrained them. For a set of $\bar{s}^{\mu\nu}$ to be consistent with observations, all twenty-seven tests have to be passed within observational uncertainties. This reduces correlations between the components of $\bar{s}^{\mu\nu}$ numerously. Figure 8 illustrated the values and distributions of $\bar{s}^{\mu\nu}$ that pass all tests in the sim-

ulation [87]; see the second column in Table 1 for statistical numbers. These limits are very tight limits in the experimental post-Newtonian gravity [121].

As in the cases of LLR and atom interferometry, the $\bar{s}^{\rm TT}$ component does not enter the orbital dynamics of binary pulsars and spin precession of solitary pulsars, if the boost between different frames is neglected [76, 117, 120]. An idea of using the boost effect between different Lorentz frames was proposed to constrain $\bar{s}^{\rm TT}$ in the context of binary pulsar timing [120]. A full Lorentz transformation includes rotations and boosts. When the frame comoving with the binary has a relative velocity with respect to the standard frame of SME, the boost will mix the $\bar{s}^{\rm TT}$ component in the standard frame into the other components of $\bar{s}^{\mu\nu}$ in the binary-comoving frame [76, 120]. Therefore, through constraining the time-spatial and spatial-spatial components in the binary-comoving frame, one can effectively constrain the $\bar{s}^{\rm TT}$ component in the standard SME frame.

In order to use the boost, one needs to have the knowledge of 3-dimensional bulky velocity of the binary with respect to the Solar System. This is possible for the aforementioned three white dwarf – neutron star binaries with both radio and optical observations [38, 42, 43]. If one focuses on the possibility that there exists a preferred frame in SME, then the only nonvanishing component of $\bar{s}^{\mu\nu}$ is $\bar{s}^{\rm TT}$ in this preferred frame. In this case it is possible to directly constrain $\bar{s}^{\rm TT}$ even without knowing the longitude of ascending node, Ω. This was done by obtaining the limit of $\bar{s}^{\rm TT}$ as a function of Ω, and then conservatively choosing the worst one, similar to the direct test of α_1 [86].[8]

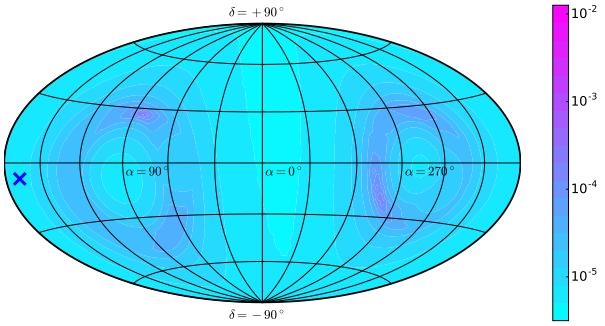

Figure 9 Combined limits on $|\bar{s}^{\rm TT}|$ from three binary pulsars for different preferred frames. Here (α, δ) denotes the movement direction of the Solar System with respect to a preferred frame. The magnitude of its velocity is assumed to be 369 km s^{-1}. The blue cross is the direction of the frame where CMB is isotropic at first-order approximation (the CMB frame). Data are taken from Ref. [120].

PSR J1738+0333 [38] turns out to be the best system to constrain the local Lorentz invariance in gravity [86, 120]. If one assumes that the CMB defines a preferred frame, then calculations gave $|\bar{s}^{\rm TT}| < 8 \times 10^{-6}$ at 68% confidence level [120]. More generally, without assuming the existence of a preferred frame, one gets $|\bar{s}^{\rm TT}| < 1.4 \times 10^{-4}$ at 68% confidence level [120].

If there exists a preferred frame that is different from the CMB frame, binary pulsars are still valuable in constraining SME. Figure 9 illustrates the concept that, because of multiple pulsar systems with different orientations, it is possible to constrain any kind of preferred-frame effects. The figure shows the combined limits that are obtained from PSRs J1738+0333, J1012+5307, and J0348+0432 for any direction of the preferred frame [120]. It is clear that with three binaries, whatever direction is the preferred frame, the local Lorentz invariance violation in SME can be constrained to a level better than 10^{-4}.

Very recently, Jennings et al. included violations of local Lorentz invariance in the gravitationally coupled matter sector and studied the possibility to constrain these matter-gravity couplings with pulsar timing experiments [111, 113]. It is an extension of the previous study by Bailey and Kostelecký where only the gravity degree was considered [76]. Because of the large degrees of freedom in parameter estimation, the practical use of a complete timing formula to a specific binary pulsar is not clear yet. A simultaneous fitting to multiple binary pulsars might help breaking some degeneracy.

Planetary Orbital Dynamics. In the course of preparing this review, Hees et al. analyzed the planetary orbital dynamics within the framework of SME. The supplementary advances of the perihelia and of the nodes obtained by planetary ephemerides analysis were used to constrain SME coefficients from the pure gravity sector and also from gravity-matter couplings [118]. The observations of Mercury, Venus, Earth-Moon barycenter,[9] Mars, Jupiter, and Saturn in INPOP10a were nicely utilized to constrain different combinations of $\bar{s}^{\mu\nu}$ and gravity-matter couplings. However, because of the small inclinations of planetary orbits with respect to each other, the limits on $\bar{s}^{\mu\nu}$ are highly correlated (see their Table II). After combining their limits with that of LLR and atom interferometry, the correlations can be vastly broken [118], and results comparable with that of pulsar timing were obtained.

In Section 4.1 and Section 4.2, only the conservative dynamics with local Lorentz invariance violation were considered. The dissipative effects, associated with gravitational radiation, can also be used to constrain local Lorentz invariance in gravity effectively; as mentioned in Section 2. Yagi et al. analyzed in detail the modification of orbital decay rate (notably with gravitational dipole radiation and quadrupole component of the emission), caused by a preferred time direction, in the khronometric theory (a possible completion is Hořava-Lifshitz gravity) and Einstein-Æther theory [46-48]. They found that the orbital evolution of bi-

[8] When $\bar{s}^{\mu\nu} = 0$ except $\bar{s}^{\rm TT} = \bar{s}^{\rm XX} + \bar{s}^{\rm YY} + \bar{s}^{\rm ZZ}$, there are three tests, namely Eqs. (33–35), that have to be satisfied for each binary pulsar. These tests are proved to compensate mutually and give decent constraints for every Ω. See Figures 2–4 in Ref. [120] for details.

[9] In the case of Earth-Moon barycenter, a full 3-body dynamics was neglected in Ref. [118] without justification.

nary pulsars depends critically on the sensitivities of the stars, which measure how their binding energies depend on the motion relative to the preferred frame. With precision measurements of orbital decay from PSRs J1141−6545, J0348+0432, J0737−3039, and J1738+0333, they were able to constrain the parameters in above two theories tightly (see e.g., Figure 2 in Ref. [46]). Thus it extends previous tests of dipole radiation in Lorentz-invariant theories [26, 128] (see Section 2) to Lorentz-violating theories.

5 Translational Symmetries and Conservation of Energy-Momentum

In this section, we will briefly discuss experimental constraints on the conservations of energy and momentum in gravity theories.

- In the SME framework, as the theory is defined by an invariant action principle, see Eq. (29), that includes no explicit spacetime dependence, translational symmetries are preserved. According to Noether's theorem, energy and momentum are conserved in SME [133].

- In the PPN framework, the violation of conservation of total momentum is described by five PPN parameters, α_3 and ζ_i $(i = 1, 2, 3, 4)$. If the action and reaction of gravitational force are equal (Newton's third law for the gravitational interaction), the momentum of the system should be conserved in the post-Newtonian limit. Therefore, the possible nonzero values of α_3 and ζ_i could imply a possible difference in the active gravitational mass (that produces the "action") and the passive gravitational mass (that receives the "action"). Therefore, we will discuss tests of momentum-conservation-violating parameters in the PPN formalism.

Among these nonconservative PPN parameters, the best constrained one is α_3. The self-acceleration effect of α_3 on binary pulsars that leads to polarization of orbit was discussed in Section 4.1. An extra acceleration, $\mathbf{a}_{\alpha_3} \propto \mathbf{v}^0 \times \mathbf{\Omega}$, see Eq. (27), that is perpendicular to the plane defined by pulsar's absolute velocity, $\mathbf{v}^0$, and spin, is constrained, and leads to a limit of $|\alpha_3|$ at the level of $O(10^{-20})$.

In the set of ζ_i's, ζ_1 was constrained indirectly through the Nordtvedt effect that describes the violation of SEP (see Section 2). The Nordtvedt parameter, $\eta_N = (m_I - m_P)/E_{\rm grav}$, describes the difference between the inertial mass, m_I, and the passive gravitational mass, m_P, normalized to the gravitational self-energy of the body, $E_{\rm grav}$. ζ_1 enters the Nordtvedt parameter together with other PPN parameters,

$$\eta_N = 4\beta - \gamma - 3 - \frac{10}{3}\xi - \alpha_1 + \frac{2}{3}\alpha_2 - \frac{2}{3}\zeta_1 - \frac{1}{3}\zeta_2 \,. \quad (37)$$

When $\beta, \gamma, \xi, \alpha_1$, and ζ_2 are constrained independently, a limit of η_N could lead to a constraint on ζ_1. As mentioned in Section 2, the best limit of η_N comes from LLR by constraining possible perturbation in the Earth-Moon distance. Because of the improvements in other PPN parameters in Eq. (37) with new experiments, the precision of ζ_1 is currently limited by the precision of η_N, and one can infer $|\zeta_1| \lesssim 10^{-3}$.

The PPN parameter ζ_2 measures how much gravity is produced by the gravitational energy [134]. Together with α_3, it produces an extra self-acceleration in direction to the periastron of a binary orbit. As a consequence, the acceleration introduces a nonvanishing value for the second time derivative of the orbital period. With the observational upper limit from PSR B1913+16, Will was able to constrain $|\alpha_3 + \zeta_2| < 4 \times 10^{-5}$ [134]. Because α_3 is constrained with much more sensitive test independently (see Section 4.1), the above limit reduces to $|\zeta_2| < 4 \times 10^{-5}$.

The PPN parameter ζ_3 produces an asymmetry between the passive gravitational mass, m_P, and the active gravitational mass, m_A, as $m_A - m_P = \frac{1}{3}\zeta_3 E_{\rm EM,static}$, where $E_{\rm EM,static}$ is the electrostatic binding energy of the body. With the Moon and the Earth well modeled, one can convert the limit of anomalous secular acceleration in the Sun-Earth-Moon dynamics from LLR into a limit of ζ_3. By this, $|\zeta_3|$ is constrained to be less than 10^{-8} [135]. One needs to keep in mind that the limit of ζ_3 could have degeneracy with a nonzero $\dot{G}/G$ [3] (see next section).

There is no direct constraint yet on the last parameter, ζ_4. Nevertheless, there is strong theoretical evidence that this parameter is dependent on other PPN parameters [136],

$$\zeta_4 = \frac{1}{2}\alpha_3 + \frac{1}{3}\zeta_1 - \frac{1}{2}\zeta_3 \,. \quad (38)$$

Such a dependence is expected because of an expected relation of the gravitational effects from kinetic energy, internal energy, and pressure of matter [3]. It is possible to estimate a limit on ζ_4 at the level of $O(10^{-3})$ from the limits of α_3, ζ_1, and ζ_3 with above relation.

To shortly summarize, GR predicts that, for an isolated gravitating system in asymptotically flat spacetime, energy and momentum are conserved[10] [17]. Various experiments proved that in the gravitational interaction, energy and momentum are conserved to a very high precision, consistent with the prediction of GR.

6 Time Varying Gravitational Constant

The locally measured Newtonian gravitational constant G may vary with time as the Universe expands. In fact, this is expected for most alternatives to GR that violate SEP [15]. For the $T_1(\alpha_0, \beta_0)$ class of scalar-tensor theories, introduced in Section 2, the temporal change in G can be expressed in

[10] With gravitational radiation, one needs to add up the amount of energy and momentum at infinity, namely, gravitational waves, through the balance equation.

terms of the time varying asymptotic scalar field $\varphi_\infty(t)$ of a local system. To linear order one finds [137],

$$\frac{\dot{G}}{G} = 2\left[1 + \frac{\beta_0}{1+\alpha_0^2}\right]\alpha_0\dot{\varphi}_\infty = \eta_N \frac{1+\alpha_0^2}{\alpha_0}\dot{\varphi}_\infty \simeq \eta_N \frac{\dot{\varphi}_\infty}{\alpha_0} , \quad (39)$$

where in the last step we have used the approximation $(1 + \alpha_0^2)/\alpha_0 \simeq 1/\alpha_0$, a consequence of the experimental evidence that $\alpha_0^2 \ll 1$. The introduction of the Nordtvedt parameter η_N in Eq. (39) illustrates nicely the connection between $\dot{G}$ and a violation of SEP. The quantity $\dot{\varphi}_0$ can be calculated from a cosmological model, and by this be linked to the Hubble constant H_0 (see for instance, Ref. [138]). More generally, one can write for the present change of G,

$$\frac{\dot{G}}{G} = \sigma H_0 , \quad (40)$$

where the value of the Hubble constant can be taken from Ref. [139], $H_0 = 67.8\,\mathrm{km\,s^{-1}\,Mpc^{-1}}$.

By now there are various experiments that tightly constrain a change in the gravitational constant on different time scales. Some of them probe a change over cosmological time scales, i.e. $G(t)$, others constrain a change of today's $\dot{G}$ (see Ref. [137] for a review).

In a binary system, a time variation of G changes the orbital period P_b. If the gravitational binding energy of the masses is small, like for Solar system bodies, the change of the orbital period is to first order given by [140],

$$\frac{\dot{P}_b}{P_b} = -\frac{\dot{n}_b}{n_b} = -2\frac{\dot{G}}{G} , \quad (41)$$

and the semimajor axis of the relative motion changes according to,

$$\frac{\dot{a}}{a} = -\frac{\dot{G}}{G} . \quad (42)$$

In the Solar system, LLR gives [141]

$$\begin{aligned}\frac{\dot{G}}{G} &= (-0.7 \pm 3.8)\times 10^{-13}\,\mathrm{yr}^{-1} \\ &= (-0.0010 \pm 0.0055)\,H_0 , \end{aligned} \quad (43)$$

and from planetary ephemerides one has [142]

$$\begin{aligned}\frac{\dot{G}}{G} &= (0.1 \pm 1.8)\times 10^{-13}\,\mathrm{yr}^{-1} \\ &= (0.0001 \pm 0.0026)\,H_0 . \end{aligned} \quad (44)$$

When one uses binary pulsars to test for a time varying gravitational constant, one has to keep in mind that Eq. (41) is not applicable to systems containing strongly self-gravitating bodies [143]. This can be made plausible by the following argument. A change in G changes the gravitational binding energy of a self-gravitating body, and by this its mass. While such a change is negligible in the Earth-Moon system, since the fractional binding energy is very small for these bodies ($\epsilon_{\mathrm{Earth}} \approx -5\times 10^{-10}$), it is significant for neutron stars, where the gravitational self-energy accounts for a significant fraction of the total mass ($\epsilon_{\mathrm{NS}} \sim -0.1$). A detailed calculation can be found in Ref. [143], which shows that for a binary pulsar system Eq. (41) has to be modified to

$$\frac{\dot{P}_b}{P_b} = -2\frac{\dot{G}}{G}\left[1 - \left(1 + \frac{m_c}{2M}\right)s_p - \left(1 + \frac{m_p}{2M}\right)s_c\right] , \quad (45)$$

where m_p and m_c denote pulsar and companion mass respectively, and $M = m_p + m_c$. The "sensitivity",

$$s_A \equiv -\left.\frac{\partial(\ln m_A)}{\partial(\ln G)}\right|_N , \quad (46)$$

measures how the mass of body A changes with a change of the local gravitational constant G, for a fixed baryon number N (see Ref. [15] for details). For a given mass, the sensitivity of a neutron star depends on the equation of state and on the specifics of the gravity theory. If the companion of the pulsar is a weakly self-gravitating star, like a white dwarf, s_c becomes negligible and Eq. (45) simplifies to

$$\frac{\dot{P}_b}{P_b} \simeq -2\frac{\dot{G}}{G}\left[1 - \left(1 + \frac{m_c}{2M}\right)s_p\right] . \quad (47)$$

The currently best pulsar limit for a change in the gravitational constant comes from the pulsar – white dwarf system, PSR J1713+0747. PSR J1713+0747 is a $1.3\,M_\odot$ millisecond pulsar, which is in a wide ($P_b = 67.8$ d) low eccentricity orbit with a $0.29\,M_\odot$ white dwarf companion. Based on 21 years of timing data for that system, Zhu et al. [98] derived,

$$\begin{aligned}\frac{\dot{G}}{G} &= (-6 \pm 11)\times 10^{-13}\,\mathrm{yr}^{-1} \\ &= (0.009 \pm 0.016)\,H_0 , \end{aligned} \quad (48)$$

with 95% confidence. It is generally expected that a gravity theory with a varying gravitational constant also predicts the existence of dipolar gravitational waves, a further consequence of SEP violation, as discussed in Section 2. The emission of dipolar radiation modifies $\dot{P}_b$, and could in principle even balance a significant part of a change in P_b caused by $\dot{G}$. In the absence of non-perturbative strong-field effects one finds for the change in the orbital period of a pulsar – white dwarf system in a small-eccentricity ($e \ll 1$) orbit the combined expression (see Ref. [42]),

$$\begin{aligned}\frac{\dot{P}_b - \dot{P}_b^{\mathrm{GR}}}{P_b} \simeq\ & -2\frac{\dot{G}}{G}\left[1 - \left(1 + \frac{m_c}{2M}\right)s_p\right] \\ & -\frac{4\pi^2}{P_b^2}\frac{Gm_pm_c}{c^3M}\kappa_D s_p^2 \quad + O(s_p^3) . \end{aligned} \quad (49)$$

The constant κ_D is a theory dependent constant, which is a priori unknown in a generic test, where no specific gravity theory is applied. As proposed in Ref. [42], it is then possible to combine two pulsars with a sufficiently large difference in their orbital periods, P_b, to constrain $\dot{G}$ and κ_D simultaneously. In Ref. [98], Zhu et al. have used PSRs J1012+5307 and J1738+0333, in combination with PSR J1713+0747 for

their analysis. This way they determined, besides the result (48), the constraint $\kappa_D = (-0.9\pm3.3)\times10^{-4}$ (95% confidence). As a final note, in such a generic test, as outlined above, one has to make certain reasonable assumptions about the value of s_A and how it changes with the pulsar mass, since the three pulsars used in Ref. [98] have quite different masses. Certain aspects of strong-field gravity related to $\dot{G}$ cannot be captured within this framework, as we will discuss below.

As one can see from Eq. (48), the pulsar limit on $\dot{G}$ is still somewhat weaker than the ones from the Solar system; see Eqs. (43) and (44). However, binary pulsar experiments are sensitive to strong-field related aspects of $\dot{G}$, which can in principle lead to an enhancement of $\dot{G}$, an effect that is not captured by the linear-in-s_A expression (47). This has been demonstrated in Ref. [20], within the $T_1(\alpha_0,\beta_0)$ class of mono-scalar-tensor theories [26,27]. Most easily this is seen, when looking at the effective gravitational constant $\mathcal{G}_{AB}$ introduced in Section 2. For the effective gravitational constant, describing the gravitational interaction between two strongly self-gravitating bodies (as measured in the physical Jordan-frame), Eq. (39) changes to,

$$\frac{\dot{\mathcal{G}}_{12}}{\mathcal{G}_{12}} = 2\left[1 + \frac{(\sigma_1/\alpha_0)\beta_2 + (\sigma_2/\alpha_0)\beta_1}{2(1+\sigma_1\sigma_2)}\right]\alpha_0\dot{\varphi}_0 \,, \qquad (50)$$

where $\beta_A = \partial\sigma_A/\partial\varphi_\infty$. For two weakly self-gravitating masses, Eq. (50) approaches Eq. (39), since $\sigma_A/\alpha_0 \to 1$ and $\beta_A \to \beta_0$. On the other hand, in the presence of significant scalarization effects in the strong gravitational fields of neutron stars, the expression in brackets of Eq. (50) can be considerably larger than the corresponding expression in Eq. (39), even for β_0 values which are not yet excluded by binary pulsar experiments (see Ref. [20]). As a conclusion, $\dot{G}$ tests with binary pulsars can be more sensitive than Solar system tests in situations where a change in the gravitational constant gets enhanced by strongly non-linear strong-field effects in neutron stars. The details depend on the specifics of the gravity theory and the mass of the neutron star.

7 Summary

At the time when Nordtvedt and Will built the parametrized post-Newtonian (PPN) formalism for post-Newtonian gravity, more than forty years ago [89], the WEP was very well examined experimentally. Position invariance and Lorentz invariance for non-gravitational physics were also well established. These empirical facts, that constitute the Einstein equivalence principle (EEP), are the foundation for the PPN formalism [15]. In the PPN formalism, post-Newtonian physics is required to comply with a metric theory of gravity which is a result of EEP. The strong equivalence principle (SEP) can be violated within the PPN formalism when PPN parameters deviate from their GR predictions. In the past few decades the PPN formalism formed the main foundation for testing gravity in the Solar system and, for some of its aspect, also for binary pulsars. Continuously accumulating data now point towards SEP at very high precision at the first post-Newtonian order. It becomes even harder today for theorists to build a gravity theory beyond GR. The new theory either needs a novel mechanism to "screen" deviations from GR in aforementioned gravity experiments, or comply with the results at the probed precision, say, by designing a gravity theory that incorporates extremely small extra couplings or that deviates from GR beginning at the second or even higher post-Newtonian orders. Even at higher orders, some effects are constrained as well, e.g., the reaction of gravitational radiation on the orbital period of a binary pulsar [20].

It seems that Einstein's general relativity (GR) is the only valid gravity theory that fully respects SEP [3]. If one loosens some requirements from SEP to extend the arena of gravity theories, it might be possible to build a new gravity theory that is able to present new features with theoretical and/or phenomenal advantages. Nevertheless, a new gravity theory must be able to conform with current existing experimental data that support SEP at exquisite precision. In this short review, we presented some modern tests of important founding principles of current wisdom in the gravity community. Well designed and well performed experiments from pulsar astronomy were highlighted, as they provide very constraining results in various aspects of gravitation, and in the meantime, encode some strong-field dynamics associated with neutron stars. For these tests, strictly speaking, some results on tests of local position invariance, local Lorentz invariance, and conservation laws of gravitation represent tests of *effective* strong-field generalizations of the (originally designed, weak-field, slow-motion) post-Newtonian gravity in PPN and SME frameworks. However, previous knowledge of strong-field dynamics hints at even tighter limits on weak-field correspondents or new limits on unprobed higher-order coefficients if strong-field contributions are explicitly taken into account. For example, if the α_2 limit obtained from pulse-profile observations of solitary pulsar [72] can be expanded with (in accordance with the expansion of the difference between inertial mass and gravitational mass, in terms of the Nordtvedt parameter η_N),

$$\alpha_2 = \alpha_2^{(0)} + \alpha_2^{(1)}\frac{E_{\rm grav}}{Mc^2} + \alpha_2^{(2)}\left(\frac{E_{\rm grav}}{Mc^2}\right)^2 + \cdots \,, \qquad (51)$$

then the limit in Eq. (26) not only constrains the weak-field counterpart, $\alpha_2^{(0)}$, at the level of $O(10^{-9})$, but also poses strong constraints on higher-order terms, $\alpha_2^{(1)}$, $\alpha_2^{(2)}$, and so on, at the levels of $O(10^{-8})$, $O(10^{-7})$, and so on, with $|E_{\rm grav}/Mc^2| \simeq 0.1$ for compact neutron stars, in particular when combined with Solar system constraints. Detailed accurate mapping of strong-field generalization and weak-field counterpart needs explicit calculations in specified gravity theories, for example, in scalar-tensor theories of Damour and Esposito-Farèse [28]. Also, equations like (51) completely fail to capture non-perturbative strong field deviations, like spontaneous scalarization [26]. To understand the meaning of pulsar limits in such situations, it is very helpful to discuss pulsars

within a theory-specific framework, like what we have done here for the $T_1(\alpha_0,\beta_0)$ class of scalar-tensor theories.

Although pulsar timing allows us to test some strong-field dynamics, in particular in the quasi-stationary strong-field regime, experiments posing a complete set of constraints on strong-field orbital dynamics of binaries are only at dawn. The upcoming gravitational wave observations from ground- and space-based detectors will undoubtedly open the window to the highly dynamical strong-field regime with typical orbital velocities of $v_{\rm orb} \sim 0.1\,c$. With the first gravitational-wave event, GW150914, detected at the Laser Interferometer Gravitational-wave Observatory (LIGO) [144], a new era for testing gravitation in strong gravitational field has started [3, 23, 145]. Tests of strong-field gravity from gravitational waves and from pulsars are complementary to each other. For example, in testing scalar-tensor theories, coalescence of neutron stars and timing of binary pulsars could probe different portion of parameter space, as well as different scenarios of scalarization (nondynamical spontaneous scalarization [101] versus dynamical scalarization [31, 146]). In the parameter space where those two kinds of observation overlap, the results from gravitational waves and from pulsar timing will be valuable for cross check. From another perspective, coalescences of compact objects provide tests based on transient events, while pulsar timing provides tests based on long term observations. It will be interesting to compare and combine the constraints from these two sets of experiments with their different characteristics, probing different gravity regimes.

We thank Renxin Xu for invitation and Weiwei Zhu for reading the manuscript. This work has made use of NASA's Astrophysics Data System.

1 A. Einstein, in *Sitzungsberichte der Königlich Preußischen Akademie der Wissenschaften* (Berlin 1915), pp. 844–847.
2 A. Einstein, in *Sitzungsberichte der Königlich Preußischen Akademie der Wissenschaften* (Berlin 1915), pp. 831–839.
3 C. M. Will, Living Rev. Relativ. **17**, 4 (2014).
4 [Particle Data Group] K. A. Olive, K. Agashe, C. Amsler, M. Antonelli, J.-F. Arguin, D. M. Asner, H. Baer, H. R. Band, R. M. Barnett, T. Basaglia, et al., Chin. Phys. C **38**, 090001 (2014).
5 S. W. Hawking and G. F. R. Ellis, *The Large Scale Structure of Space-Time* (Cambridge University Press, 1973).
6 G. Amelino-Camelia, Living Rev. Relativ. **16**, 5 (2013).
7 T. Clifton, P. G. Ferreira, A. Padilla, and C. Skordis, Phys. Rept. **513**, 1 (2012).
8 H. Goenner, Gen. Relat. Gravit. **44**, 2077 (2012).
9 P. Jordan, *Schwerkraft und Weltall* (Vieweg, Braunschweig, 1955).
10 J. D. Bekenstein, Phys. Rev. D **70**, 083509 (2004).
11 J. D. Bekenstein, Phys. Rev. D **71**, 069901 (2005).
12 P. Hořava, Phys. Rev. D **79**, 084008 (2009).
13 D. Blas, O. Pujolàs, S. Sibiryakov, J. High Energy Phys. **04**, 018 (2011).
14 E. Berti, E. Barausse, V. Cardoso, L. Gualtieri, P. Pani, U. Sperhake, L. C. Stein, N. Wex, K. Yagi, T. Baker, et al., Class. Quantum Grav. **32**, 243001 (2015).
15 C. M. Will, *Theory and Experiment in Gravitational Physics* (Cambridge University Press, Cambridge, 1993).
16 T. Damour, In *Physics of Relativistic Objects in Compact Binaries: From Birth to Coalescence*, edited by M. Colpi, P. Casella, V. Gorini, U. Moschella, and A. Possenti (Astrophysics and Space Science Library, Volume 359, 2009), pp. 1–41.
17 C. W. Misner, K. S. Thorne, and J. A. Wheeler, *Gravitation* (W. H. Freeman and Company, San Francisco, 1973).
18 E. Di Casola, S. Liberati, and S. Sonego, Am. J. Phys. **83**, 39 (2015).
19 I. H. Stairs, Living Rev. Relativ. **6**, 5 (2003).
20 N. Wex, in *Brumberg Festschrift*, edited by S. M. Kopeikein (de Gruyter, Berlin, 2014).
21 V. A. Kostelecký, Phys. Rev. D **69**, 105009 (2004).
22 B. S. Sathyaprakash and B. F. Schutz, Living Rev. Relativ. **12**, 2 (2009).
23 A. Buonanno and B. S. Sathyaprakash, in *General Relativity and Gravitation: A Centennial Perspective*, edited by A. Ashtekar, B. K. Berger, J. Isenberg, and M. A. H. MacCallum, in press, arXiv:1410.7832
24 K. Nordtvedt, Phys. Rev. **170**, 1186 (1968).
25 J. Müller, F. Hofmann, and L. Biskupek, Class. Quantum Grav. **29**, 184006 (2012).
26 T. Damour and G. Esposito-Farèse, Phys. Rev. Lett. **70**, 2220 (1993).
27 T. Damour and G. Esposito-Farèse, Phys. Rev. D **53**, 5541 (1996).
28 T. Damour and G. Esposito-Farèse, Class. Quantum Grav. **9**, 2093 (1992).
29 T. Damour, In *Three Hundred Years of Gravitation*, edited by S.W. Hawking and W. Israel (Cambridge University Press, Cambridge; New York, 1987), pp. 128–198.
30 J. M. Lattimer and M. Prakash, Astrophys. J. **550**, 426 (2001).
31 M. Shibata, K. Taniguchi, H. Okawa, and A. Buonanno, Phys. Rev. D **89**, 084005 (2014).
32 T. Damour and G. Schäfer, Phys. Rev. Lett. **66**, 2549 (1991).
33 I. H. Stairs, A. J. Faulkner, A. G. Lyne, M. Kramer, D. R. Lorimer, M. A. McLaughlin, R. N. Manchester, G. B. Hobbs, F. Camilo, A. Possenti, et al., Astrophys. J. **632**, 1060 (2005).
34 M. E. Gonzalez, I. H. Stairs, R. D. Ferdman, P. C. C. Freire, D. J. Nice, P. B. Demorest, S. M. Ransom, M. Kramer, F. Camilo, G. Hobbs, et al., Astrophys. J. **743**, 102 (2011).
35 P. C. C. Freire, M. Kramer, and N. Wex, Class. Quantum Grav. **29**, 184007 (2012).
36 S. M. Ransom, I. H. Stairs, A. M. Archibald, J. W. T. Hessels, D. L. Kaplan, M. H. van Kerkwijk, J. Boyles, A. T. Deller, S. Chatterjee, A. Schechtman-Rook, et al., Nature **505**, 520 (2014).
37 L. Shao, Phys. Rev. D 93, 084023 (2016).
38 P. C. C. Freire, N. Wex, G. Esposito-Farèse, J. P.W. Verbiest, M. Bailes, B. A. Jacoby, M. Kramer, I. H. Stairs, J. Antoniadis, and G. H. Janssen, Mon. Not. R. Astron. Soc. **423**, 3328 (2012).
39 M. Kramer and N. Wex, Class. Quantum Grav. **26**, 073001 (2009).
40 S. Mirshekari and C. M. Will, Phys. Rev. D **87**, 084070 (2013).
41 N. D. R. Bhat, M. Bailes, and J. P. W. Verbiest, Phys. Rev. D **77**, 124017 (2008).
42 K. Lazaridis, N. Wex, A. Jessner, M. Kramer, B. W. Stappers, G. H. Janssen, G. Desvignes, M. B. Purver, I. Cognard, G. Theureau, et al., Mon. Not. R. Astron. Soc. **400**, 805 (2009).
43 J. Antoniadis, P. C. C. Freire, N. Wex, T. M. Tauris, R. S. Lynch, M. H. van Kerkwijk, M. Kramer, C. Bassa, V. S. Dhillon, T. Driebe, et al., Science **340**, 448 (2013).
44 G. Desvignes, R. N. Caballero, L. Lentati, et al., Mon. Not. R. Astron. Soc., **458**, 3341 (2016).
45 J.-M. Gérard and Y. Wiaux, Phys. Rev. D **66**, 024040 (2002).
46 K. Yagi, D. Blas, E. Barausse, and N. Yunes, Phys. Rev. Lett. **112**,

161101 (2014).
47 K. Yagi, D. Blas, E. Barausse, and N. Yunes, Phys. Rev. D **89**, 084067 (2014).
48 K. Yagi, D. Blas, E. Barausse, and N. Yunes, Phys. Rev. D **90**, 069902 (2014).
49 H. Lichtenegger and B. Mashhoon, in *The Measurement of Gravitomagnetism: A Challenging Enterprise*, edited by L. Iorio (Nova Science, New York, 2007), pp. 13–25.
50 W. Rindler, Phys. Lett. A **187** 236 (1994).
51 M. Fierz, Helv. Phys. Acta **29** 128 (1956).
52 C. Brans and R. H. Dicke, Phys. Rev. **124**, 925 (1961).
53 J. B. Barbour and H. Pfister (eds.), *Mach's Principle: From Newton's Bucket to Quantum Gravity* (Boston: Birkhäuser, 1995).
54 H. Bondi and J. Samuel, Phys. Lett. A **228**, 121 (1997).
55 A. N. Whitehead, *The Principle of Relativity* (Cambridge: Cambridge University Press, 1922).
56 D. W. Sciama, Mon. Not. R. Astron. Soc. **113**, 34 (1953).
57 C. M. Will, Astrophys. J. **185**, 31 (1973).
58 D. J. Raine, Mon. Not. R. Astron. Soc. **171**, 507 (1975).
59 G. Gibbons and C. M. Will, Stud. Hist. Phil. Sci. **39**, 41 (2008).
60 G. Cocconi and E. Salpeter, Nuovo Cimento **10**, 646 (1958).
61 G. Cocconi and E. Salpeter, Phys. Rev. Lett. **4**, 176 (1960).
62 L. Shao and N. Wex, Class. Quantum Grav. **30**, 165020 (2013).
63 L. Shao, N. Wex, and M. Kramer, in *Proceedings of the Thirteenth Marcel Grossmann Meeting on General Relativity*, edited by K. Rosquist, R. T. Jantzen, R. Ruffini (Singapore: World Scientifici, 2015), pp. 1704–1706.
64 K. Nordtvedt, Astrophys. J. **320**, 871 (1987).
65 K. Nordtvedt and C. M. Will, Astrophys. J. **177**, 775 (1972).
66 R. J. Warburton and J. M. Goodkind, Astrophys. J. **208**, 881 (1976).
67 S. Shiomi, Prog. Theor. Phys. Suppl. **172**, 61 (2008).
68 D. R. Lorimer and M. Kramer, *Handbook of Pulsar Astronomy* (Cambridge: Cambridge University Press, 2004).
69 B. A. Archinal, M. F. A'Hearn, E. Bowell, A. Conrad, G. J. Consolmagno, R. Courtin, T. Fukushima, D. Hestroffer, J. L. Hilton, G. A. Krasinsky, et al., Celest. Mech. Dyn. Astr. **109**, 101 (2009).
70 L. Iorio, Mon. Not. R. Astron. Soc. **437**, 3482 (2014).
71 A. Skumanich, Astrophys. J. **171**, 565 (1972).
72 L. Shao, R. N. Caballero, M. Kramer, N. Wex, D. J. Champion, and A. Jessner, Class. Quantum Grav. **30**, 165019 (2013).
73 L. Guillemot, T. J. Johnson, C. Venter, M. Kerr, B. Pancrazi, M. Livingstone, G. H. Janssen, P. Jaroenjittichai, M. Kramer, I. Cognard, et al., Astrophys. J. **744**, 33 (2012).
74 J. Gil, P. Gronkowski, and W. Rudnicki, Astron. Astrophys. **132**, 312 (1984).
75 T. Jacobson and D. Mattingly, Phys. Rev. D **64**, 024028 (2001).
76 Q. G. Bailey and V. A. Kostelecký, Phys. Rev. D **74**, 045001 (2006).
77 D. Blas and E. Lim, Int. J. Mod. Phys. D **23**, 1443009 (2014).
78 J. D. Tasson, Rep. Prog. Phys. **77**, 062901 (2014).
79 V. A. Kostelecký and S. Samuel, Phys. Rev. D **39**, 683 (1989).
80 V. A. Kostelecký and S. Samuel, Phys. Rev. D **40**, 1886 (1989).
81 R. Gambini and J. Pullin, Phys. Rev. D **59**, 124021 (1999).
82 J. C. Long and V. A. Kostelecký, Phys. Rev. D **91**, 092003 (2015).
83 A. R. Solomon and J. D. Barrow, Phys. Rev. D **89**, 024001 (2014).
84 T. Damour and G. Esposito-Farèse, Phys. Rev. D **46**, 4128 (1992).
85 D. R. Lorimer, Living Rev. Relativ. **11**, 8 (2008).
86 L. Shao and N. Wex, Class. Quantum Grav. **29**, 215018 (2012).
87 L. Shao, Phys. Rev. Lett. **112**, 111103 (2014).
88 R. N. Manchester, Int. J. Mod. Phys. D **24**, 1530018 (2015).
89 C. M. Will and K. Nordtvedt, Astrophys. J. **177**, 757 (1972).
90 Y. Fujii and K. I. Maeda, *The ScalarTensor Theory of Gravitation* (Cambridge: Cambridge University Press, 2003).
91 J. F. Bell, F. Camilo, and T. Damour, Astrophys. J. **464**, 857 (1996).
92 N. Wex, in *IAU Colloq. 177: Pulsar Astronomy — 2000 and Beyond*, edited by M. Kramer, N. Wex and R. Wielebinski (Astronomical Society of the Pacific Conference Series, Volume 202, 2000), pp. 113–116.
93 N. Wex and M. Kramer, Mon. Not. R. Astron. Soc. **380**, 455 (2007).
94 M. Kramer, I. H. Stairs, R. N. Manchester, M. A. McLaughlin, A. G. Lyne, R. D. Ferdman, M. Burgay, D. R. Lorimer, A. Possenti, N. D'Amico, et al., Science **314**, 97 (2006).
95 T. Damour and K. Nordtvedt, Phys. Rev. Lett. **70**, 2217 (1993).
96 J. Müller, J. G. Williams, and S. G. Turyshev, in *Lasers, Clocks and Drag-Free Control: Exploration of Relativistic Gravity in Space*, edited by H. Dittus, C. Lämmerzahl, and S. G. Turyshev (Astrophysics and Space Science Library, Volume 349, 2008), pp. 457–472.
97 J. F. Bell and T. Damour, Class. Quantum Grav. **13**, 3121 (1996).
98 W. W. Zhu, I. H. Stairs, P. B. Demorest, D. J. Nice, J. A. Ellis, S. M. Ransom, Z. Arzoumanian, K. Crowter, T. Dolch, R. D. Ferdman, et al., Astrophys. J. **809**, 41 (2015).
99 D. Hilbert, in *Königliche Gesellschaft der Wissenschaften zu Göttingen. Mathematisch-physikalische Klasse* (Nachrichten, 1916), pp. 395–407.
100 T. Damour and G. Esposito-Farèse, Phys. Rev. D **54**, 1474 (1996).
101 T. Damour and G. Esposito-Farèse, Phys. Rev. D **58**, 042001 (1998).
102 D. Colladay and V. A. Kostelecký, Phys. Rev. D **55**, 6760 (1997).
103 D. Colladay and V. A. Kostelecký, Phys. Rev. D **58**, 116002 (1998).
104 P. W. Higgs, Rev. Mod. Phys. **86**, 851 (2014).
105 F. Englert, Rev. Mod. Phys. **86**, 843 (2014).
106 Y. Bonder, Phys. Rev. D **91**, 125002 (2015).
107 R. Bluhm, Phys. Rev. D **91**, 065034 (2015).
108 K. Nordtvedt, Phys. Rev. D **14**, 1511 (1976).
109 Q. G. Bailey, V. A. Kostelecký, and R. Xu, Phys. Rev. D **91**, 022006 (2015).
110 C.-G. Shao, Y.-J. Tan, W.-H. Tan, S.-Q. Yang, J. Luo, and M. E. Tobar, Phys. Rev. D **91**, 102007 (2015).
111 V. A. Kostelecký and J. D. Tasson, Phys. Rev. D **83**, 016013 (2011).
112 S. Liberati, Class. Quantum Grav. **30**, 133001 (2013).
113 R. J. Jennings, J. D. Tasson, and S. Yang, Phys. Rev. D **92**, 125028 (2015).
114 J. B. R. Battat, J. F. Chandler, and C. W. Stubbs, Phys. Rev. Lett. **99**, 241103 (2007).
115 H. Müller, S.-W. Chiow, S. Herrmann, S. Chu, and K.-Y. Chung, Phys. Rev. Lett. **100**, 031101 (2008).
116 K.-Y. Chung, S.-W. Chiow, S. Herrmann, S. Chu, and H. Müller, Phys. Rev. D **80**, 016002 (2009).
117 Q. G. Bailey, R. D. Everett, and J. M. Overduin, Phys. Rev. D **80**, 102001 (2013).
118 A. Hees, Q.G. Bailey, C. Le Poncin-Lafitte, A. Bourgoin, A. Rivoldini, B. Lamine, F. Meynadier, C. Guerlin, and P. Wolf, Phys. Rev. D **92**, 064049 (2015).
119 Y. Xie, Res. Astron. Astrophys. **13**, 1 (2013).
120 L. Shao, Phys. Rev. D **90**, 122009 (2014).
121 V. A. Kostelecký and N. Russell, Rev. Mod. Phys. **83**, 11 (2011).
122 P. L. Bender, D. G. Currie, S. K. Poultney, C. O. Alley, R. H. Dicke, D. T. Wilkinson, D. H. Eckhardt, J. E. Faller, W. M. Kaula, J. D. Mulholland, et al., Science **182**, 229 (1973).
123 M. Kasevich and S. Chu, Phys. Rev. Lett. **67**, 181 (1991).
124 S. Chu, Nature **416**, 206 (2002).
125 C. W. F. Everitt, D. B. DeBra, B. W. Parkinson, J. P. Turneaure, J. W. Conklin, M. I. Heifetz, G. M. Keiser, A. S. Silbergleit, T. Holmes, J. Kolodziejczak, et al., Phys. Rev. Lett. **106**, 221101 (2011).
126 J. M. Overduin, Class. Quantum Grav. **32**, 224003 (2015).

127 T. Damour and N. Deruelle, Ann. Inst. Henri Poincaré A **44**, 263 (1986).

128 T. Damour and J. H. Taylor, Phys. Rev. D **45**, 1840 (1992).

129 G. Hobbs, Class. Quantum Grav. **30**, 224007 (2013).

130 M. A. McLaughlin, Class. Quantum Grav. **30**, 224008 (2013).

131 M. Kramer and D. J. Champion, Class. Quantum Grav. **30**, 224009 (2013).

132 R. N. Manchester, Class. Quantum Grav. **30**, 224010 (2013).

133 K. S. Thorne, D. L. Lee, and A. P. Lightman, Phys. Rev. D **7**, 3563 (1973).

134 C. M. Will, Astrophys. J. **393**, 59 (1992).

135 D. F. Bartlett and D. van Buren, Phys. Rev. Lett. **57**, 21 (1986).

136 C. M. Will, Astrophys. J. **204**, 224 (1976).

137 J.-P. Uzan, Living Rev. Relativ. **14**, 2 (2011).

138 S. Weinberg, *Gravitation and Cosmology: Principles and Applications of the General Theory of Relativity* (John Wiley & Sons, 1972).

139 [Planck Collaboration] P. A. R. Ade, N. Aghanim, M. I. R. Alves, C. Armitage-Caplan, M. Arnaud, M. Ashdown, F. Atrio-Barandela, J. Aumont, H. Aussel, C. Baccigalupi, et al., Astron. Astrophys. **571**, 48 (2014).

140 T. Damour, G. W. Gibbons, and J. H. Taylor, Phys. Rev. Lett. **61**, 1151 (1988).

141 F. Hofmann, J. Müller, and L. Biskupek, Astron. Astrophys. **522**, L5 (2010).

142 A. Fienga, J. Laskar, P. Exertier, H. Manche, and M. Gastineau, ArXiv preprint, arXiv:1409.4932 (2014).

143 K. Nordtvedt, Phys. Rev. Lett. **65**, 953 (1990).

144 The LIGO Scientific Collaboration and the Virgo Collaboration, Phys. Rev. Lett. **116**, 061102 (2016).

145 N. Yunes and X. Siemens, Living Rev. Relativ. **16**, 9 (2013).

146 E. Barausse, C. Palenzuela, M. Ponce, L. Lehner, Phys. Rev. D **87**, 081506 (2013).